Chromium Oxide Tetrafluoride and Its Reactions with Xenon Hexafluoride; the [XeF$_5$]$^+$ and [Xe$_2$F$_{11}$]$^+$ Salts of the [Cr^{VI}OF$_5$]$^-$, [Cr^{IV}F$_6$]$^{2-}$, [Cr^{V}OF$_5$]$^{2-}$, and [Cr$^V_2$O$_2$F$_8$]$^{2-}$ Anions

Daniel G. Stuart, Mark R. Bortolus, James T. Goettel, Hélène P. A. Mercier, and

Gary J. Schrobilgen*

Department of Chemistry, McMaster University, Hamilton, Ontario L8S 4M1, Canada

* Author to whom correspondence should be addressed. E-mail: schrobil@mcmaster.ca

ABSTRACT

Molten mixtures of XeF$_6$ and Cr^{VI}OF$_4$ in 1:1 and 1:2 molar ratios undergo reduction to Cr(V) and Cr(IV) by means of F$_2$ elimination to form [XeF$_5$][Xe$_2$F$_{11}$][Cr^{V}OF$_5$]·2Cr^{VI}OF$_4$ and [XeF$_5$]$_2$[Cr^{IV}F$_6$]·2Cr^{VI}OF$_4$, respectively, as shown by low-temperature (LT) single-crystal X-ray diffraction (SCXRD). A LT Raman spectroscopic study of an equimolar mixture of solid XeF$_6$ and CrOF$_4$ and its melt showed that [Cr^{VI}OF$_5$]$^-$ is formed as an intermediate. Reaction of [XeF$_5$]$_2$[Cr^{IV}F$_6$]·2Cr^{VI}OF$_4$ with XeF$_6$ in a melt gave [Xe$_2$F$_{11}$]$_2$[Cr^{IV}F$_6$] and [XeF$_5$]$_2$[Cr$^V_2$O$_2$F$_8$]. Their LT crystal structures revealed that [XeF$_5$]$^+$ and [Xe$_2$F$_{11}$]$^+$ are coordinated to their respective [CrF$_6$]$^{2-}$ and [Cr$_2$O$_2$F$_8$]$^{2-}$ anions by means of Xe---F–Cr bridges to form infinite chain structures. The reactions of a 1:1 molar ratio of XeF$_6$ and CrOF$_4$ in anhydrous hydrogen fluoride (aHF) and in mixed CFCl$_3$/aHF solvents yielded [XeF$_5$]$_2$[Cr$^V_2$O$_2$F$_8$]·2HF and a mixture of [XeF$_5$]$_2$[Cr$^V_2$O$_2$F$_8$]·2HF and [XeF$_5$]$_2$[Cr$^V_2$O$_2$F$_8$]·2XeOF$_4$, respectively. The SCXRD structures of the latter and aforementioned salts provide the first X-ray structures of [CrOF$_5$]$^{2-}$ and [Cr$_2$O$_2$F$_8$]$^{2-}$. The [XeF$_5$]$_2$[Cr$^V_2$O$_2$F$_8$]·2XeOF$_4$ and [XeF$_5$][Xe$_2$F$_{11}$][Cr^{V}OF$_5$]·2Cr^{VI}OF$_4$ salts were also characterized by LT Raman spectroscopy. Quantum-chemical calculations were carried out to obtain the energy-minimized, gas-phase geometries and vibrational frequencies for [Cr^{VI}OF$_5$]$^-$, [XeF$_5$]$_2$[Cr$^V_2$O$_2$F$_8$]·2XeOF$_4$, [Cr$^V_2$O$_2$F$_8$]$^{2-}$, [XeF$_5$][Xe$_2$F$_{11}$][Cr^{V}OF$_5$]·2Cr^{VI}OF$_4$, [Cr^{V}OF$_5$]$^{2-}$, and to aid in the assignments of their vibrational frequencies.

1

INTRODUCTION

The known chromium(VI) oxide fluorides were limited to CrO_2F_2,[1] $CrOF_4$,[2] the $[CrOF_5]^-$ anion,[2,3] and most recently, several $CrOF_4$ complexes with NgF_2 (Ng = Kr, Xe).[4] The existence of CrF_6 had been disputed for several decades,[5–7] however the controversy was resolved by Willner *et al.* when it was conclusively shown by matrix-isolation IR that the vibrational spectrum previously attributed to CrF_6 was, in fact, that of CrF_5.[8] A more recent matrix-isolation IR and computational study[9] is in accordance with the conclusions of Willner *et al.*[9]

Tungsten and molybdenum oxide tetrafluoride were first synthesized and described in 1907, but it was not until 1963 that the synthesis of $CrOF_4$ was reported,[10] and was subsequently improved upon to provide higher yields.[2,3] Although $[WOF_5]^{-}$[11,12] and $[MoOF_5]^-$,[11–13] have been the subject of several studies, there is a dearth of information on the $[CrOF_5]^-$ anion. The anion was synthesized as its Cs^+ salt by heating a 1:1 molar ratio of CsF and $CrOF_4$ to 100 °C in a sealed Monel reaction vessel (eq 1).[2] Elemental analysis and the IR spectrum of the product were in good agreement with the formulation, $[Cs][CrOF_5]$. The $[NO]^+$ salt was subsequently prepared by reaction of $CrOF_4$ with NOF at room temperature to give $[NO][CrOF_5]$ (eq 1).[3] The salt was characterized by low-temperature IR and Raman

$$MF \ + \ CrOF_4 \ \longrightarrow \ [M][CrOF_5] \quad M = Cs^+ \text{ or } [NO]^+ \tag{1}$$

spectroscopy and the spectrum of $[CrOF_5]^-$ was assigned under C_{4v} point symmetry.[3] Both salts were subsequently synthesized by reaction of CrO_2F_2 with either NOF or CsF at 80 °C in the presence of elemental fluorine (eq 2).[14] To date, no crystal structure of a $[CrOF_5]^-$ salt has been reported. Controlled pyrolysis of $[NO][CrOF_5]$ resulted in a mixture which was shown to be $[NO][CrOF_5]$ and $[NO][CrOF_5] \cdot nCrOF_4$ by IR spectroscopy and suggested that salts like $[NO][Cr_2O_2F_9]$ would be thermally more stable than $[NO][CrOF_5]$.[3]

$$MF \; + \; CrO_2F_2 \; + F_2 \; \longrightarrow \; [M][CrOF_5] \; + \frac{1}{2} O_2 \quad M = Cs^+ \; or \; [NO]^+ \qquad (2)$$

The chemistry of Cr(V) oxide fluorides is also limited. The preparation and vibrational spectra of $CrOF_3$ were reported in 1982,[15] and its crystal structure, along with an improved synthesis, were reported in 1985.[16] The characterizations of the K^+ and Cs^+ salts of $[Cr^VOF_4]^-$ by mass balance measurements,[17] X-ray powder diffraction,[15] infrared spectroscopy,[18] and UV-vis spectroscopy[18] have also been reported. A low-temperature ESR study of $K[CrOF_4]$ reported the observation of both $[CrOF_4]^-$ and $[CrOF_5]^{2-}$ in frozen 48% HF glasses.[19] To date, there have been no crystal structures reported for the $[CrOF_4]^-$ and $[CrOF_5]^{2-}$, or dinuclear Cr(V) oxide fluoride anions, $[Cr_2O_2F_9]^-$ and $[Cr_2O_2F_8]^{2-}$.

The noble-gas difluorides, NgF_2 (Ng = Kr, Xe), are sufficiently fluoro-basic to form adducts with the group 6 d^0 metal oxide tetrafluorides, MOF_4 (M = Cr, Mo, W), having the general formula $NgF_2 \cdot nMOF_4$ (n = 1, 2). Members of the MOF_4 series are intermediate-strength fluoride ion acceptors which do not fully transfer fluoride ion to form $[NgF][MOF_5]$ salts.[4] Instead, these adducts contain terminally coordinated NgF_2 molecules that are bonded through F–Ng–F---M bridges. Xenon hexafluoride is more fluorobasic than XeF_2,[20] and is more likely to donate fluoride ion to $CrOF_4$ to form $[XeF_5]^+$ and $[Xe_2F_{11}]^+$ salts of $[CrOF_5]^-$. Moreover, the +6 oxidation states of Xe in $[XeF_5]^+$ and $[Xe_2F_{11}]^+$ provide the strongly oxidizing reaction conditions that are required to stabilize high-oxidation state transition-metal anions, as shown by the syntheses and stabilization of the Os(VIII) salts, $[XeF_5][OsO_3F_3]$, $[Xe_2F_{11}][fac\text{-}OsO_3F_3]$, and $[XeF_5][\mu\text{-}F(OsO_3F_2)_2]$.[21]

A prior attempt to synthesize Cr(V) fluoro-anions by use of XeF_6 as a fluoride ion donor led to Cr(V) reduction and F_2 elimination.[22] Instead of the anticipated $[XeF_5][Cr^VF_6]$ salt, the reaction of XeF_6 with CrF_5 yielded $[XeF_5][Cr^{IV}F_5]$ which was characterized by single-crystal X-ray diffraction (eq 3).[22]

$$XeF_6 + CrF_5 \longrightarrow [XeF_5][CrF_5] + \tfrac{1}{2}F_2 \tag{3}$$
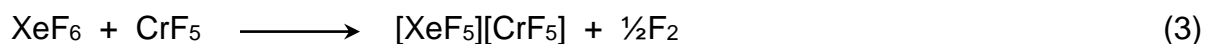
In the present study, the reactions of XeF_6 and $CrOF_4$ were investigated in molten mixtures and in the oxidatively resistant solvents, aHF and $CFCl_3$. The products were structurally characterized by low-temperature, single-crystal X-ray diffraction, and Raman spectroscopy. Quantum-chemical calculations were employed to aid in the vibrational frequency assignments and to assess the bonding in several key compounds.
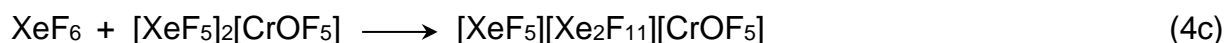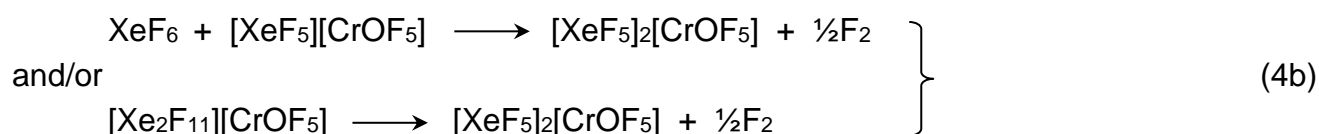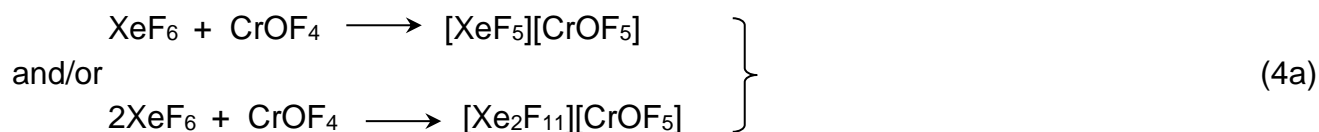
RESULTS AND DISCUSSION

Syntheses

[XeF5][Xe2F11][CrOF5]·2CrOF4 (6). The room-temperature reaction of equimolar mixtures of XeF_6 and $CrOF_4$ was initially accompanied by vigorous gas evolution and the formation of a dark purple liquid (eq 4). Fluorine gas evolution was verified by rapid tarnishing of a drop of elemental mercury at −78 °C upon exposure to the volatile reaction products. Slow cooling of the reaction mixture from 20 to 0 °C resulted in the formation of large, rod-shaped crystals (m.p. 18 °C) which were shown to be $[XeF_5][Xe_2F_{11}][CrOF_5] \cdot 2CrOF_4$ (**6**) (see X-ray Crystallography). The proposed overall reaction of XeF_6 and $CrOF_4$ in the melt at ambient temperature is given by eq 4:

$$3XeF_6 + 3CrOF_4 \xrightarrow[\text{RT}]{\text{melt}} [XeF_5][Xe_2F_{11}][CrOF_5] \cdot 2CrOF_4 + \tfrac{1}{2}F_2 \tag{4}$$

and likely proceeds by the following pathway (eqs 4a-4c):

$$XeF_6 + CrOF_4 \longrightarrow [XeF_5][CrOF_5]$$
and/or
$$2XeF_6 + CrOF_4 \longrightarrow [Xe_2F_{11}][CrOF_5] \tag{4a}$$

$$XeF_6 + [XeF_5][CrOF_5] \longrightarrow [XeF_5]_2[CrOF_5] + \tfrac{1}{2}F_2$$
and/or
$$[Xe_2F_{11}][CrOF_5] \longrightarrow [XeF_5]_2[CrOF_5] + \tfrac{1}{2}F_2 \tag{4b}$$

$$XeF_6 + [XeF_5]_2[CrOF_5] \longrightarrow [XeF_5][Xe_2F_{11}][CrOF_5] \tag{4c}$$

Co-crystallized $CrOF_4$ is introduced into the coordination sphere of $[CrOF_5]^{2-}$ upon crystallization (see compound (**6**), X-ray Crystallography).

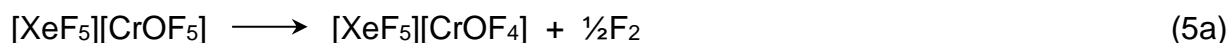In an effort to determine if $[CrOF_5]^-$ salts are formed as intermediates (eqs 4a and 4b), equimolar amounts of solid XeF_6 and $CrOF_4$ were mixed at -78 °C. Upon warming the red-colored mixture to -50 °C, the color changed to orange. Thereafter, the mixture was successively warmed to higher temperatures in steps (-30 °C to ambient temperature) and allowed to react for varying lengths of time, with intermittent agitation, followed by quenching of the sample after each warming period to -196 °C. Reaction progress was monitored by recording the low-temperature Raman spectrum after each warm/quench cycle (see footnotes, Table S1).

The Raman spectra of the orange solids (Table S1) showed that bands corresponding to free $CrOF_4$ persisted until ambient temperature was attained. Upon increasing reaction temperature a new set of bands grew until the sample was allowed to react at ambient temperature. These new bands are assigned to the $[CrOF_5]^-$ anion (eq 4a) by comparison with the known $Cs[CrOF_5]$ [2] and $[NO][CrOF_5]$ [3] salts (Table S1): $\nu(Cr\text{-}O)$, 951 cm^{-1}; $\nu_s(Cr\text{-}F_{4e})$, 640 cm^{-1}; $\nu_{as}(Cr\text{-}F_{4e})$, 568 cm^{-1}; $\nu(Cr\text{-}F_{ax})$, 527 cm^{-1}; $\delta_{umb}(CrF_{4e})$, 407 and 419 cm^{-1}; $[\delta(OCrF_e) + \delta(F_eCrF_{ax})]$, 341 cm^{-1}; $[\delta(F_eCrF_e) + \delta(F_eCrF_e)]$, 313 cm^{-1}; $[\rho_w(OCrF_{ax}) + \rho_w(F_eCrF_e)]$, 275 cm^{-1}. Other bands, which also concurrently grew in, are assigned to $[Xe_2F_{11}]^+$ by comparison with known $[Xe_2F_{11}]^+$ salts.[21,23] When the sample was briefly fused at 18 °C and immediately quenched at -196 °C, weak bands due to $[XeF_5][Xe_2F_{11}][CrOF_5]\cdot2CrOF_4$ (**6**) (see Raman Spectroscopy) began to appear in addition to the aforementioned $[Xe_2F_{11}]^+$, $[CrOF_5]^-$, and free $CrOF_4$ bands. When the latter sample was warmed to ambient temperature the sample melted with no visible sign of gas evolution. After reacting for ca. 1 min at ambient temperature and quenching at -196 °C, the Raman

4

spectrum showed $[Xe_2F_{11}][CrOF_5]$, an increased amount of compound (**6**), and no free $CrOF_4$. Continued reaction for ca. one hour at ambient temperature resulted in F_2 evolution and compound (**6**) along with a small amount of undecomposed $[Xe_2F_{11}][CrOF_5]$. Crystals of $[Xe_2F_{11}][CrOF_5]$ that were suitable for an X-ray crystal structure determination were not obtained in the course of these studies.

***$[XeF_5]_2[CrF_6]\cdot2CrOF_4$ (1).*** Approximately 1.5 equivalents of $CrOF_4$ were allowed to react with one equivalent of XeF_6 at room temperature, which yielded a dark purple-colored liquid that contained undissolved $CrOF_4$. The reaction mixture was warmed to approximately 60 °C and the contents were agitated to effect dissolution of the remaining $CrOF_4$ (eq 5). Upon slow cooling of the melt to room temperature, dark red, needle-shaped crystals of $[XeF_5]_2[CrF_6]\cdot2CrOF_4$ deposited on the walls of the reaction vessel.

The proposed pathway for the reaction of XeF_6 with $CrOF_4$ (eq 5) at elevated temperature (60 °C) initially proceeds via eq 4a to give $[XeF_5][CrOF_5]$, which then undergoes F_2 elimination (eq 5a) to form $[XeF_5][CrOF_4]$. The latter salt undergoes fluorine/oxygen metathesis with XeF_6 according to eq 5b. Co-crystallized $CrOF_4$ is likely introduced into the coordination sphere of $[CrF_6]^{2-}$ upon crystallization of the melt (see compound (**1**) in X-ray Crystallography).
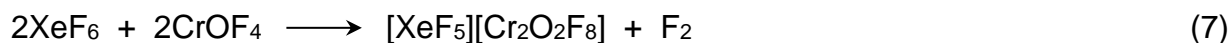
$$3XeF_6 + 3CrOF_4 \xrightarrow[\text{60 °C}]{\text{melt}} [XeF_5]_2[CrF_6]\cdot2CrOF_4 + \tfrac{1}{2}F_2 + XeOF_4 \qquad (5)$$

$$[XeF_5][CrOF_5] \longrightarrow [XeF_5][CrOF_4] + \tfrac{1}{2}F_2 \qquad (5a)$$

$$2XeF_6 + [XeF_5][CrOF_4] \longrightarrow [XeF_5]_2[CrF_6] + XeOF_4 \qquad (5b)$$

$[Xe_2F_{11}]_2[CrF_6]$ (2) and $[XeF_5]_2[Cr_2O_2F_8]$ (3). Approximately four equivalents of XeF_6 were allowed to react with one equivalent of $[XeF_5]_2[CrF_6]\cdot2CrOF_4$ in a melt at 30 °C. Slow cooling from 30 °C to room temperature led to crystalline $[Xe_2F_{11}]_2[CrF_6]$ (colorless needles) and red-$[XeF_5]_2[Cr_2O_2F_8]$ (red-orange blocks).

The reactions leading to the formation of (**2**) and (**3**) are summarized by eqs (**6**) and (**7**), respectively. Compound (**2**) arises from the addition of XeF_6 to $[XeF_5]^+$ of the starting compound, $[XeF_5]_2[CrF_6] \cdot 2CrOF_4$ (**1**) in eq 6.

$$2XeF_6 + [XeF_5]_2[CrF_6] \cdot 2CrOF_4 \xrightarrow[\text{30 °C}]{\text{melt}} [Xe_2F_{11}]_2[CrF_6] + 2CrOF_4 \qquad (6)$$
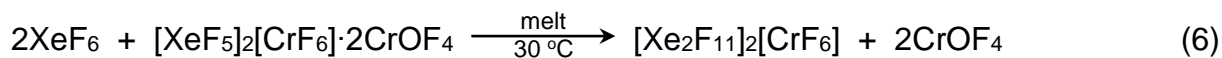
Compund (**3**) is formed by the reaction of the co-crystallized $CrOF_4$ of compound (**1**) with XeF_6 (eq 7). The overall reaction presumably occurs by two consecutive reactions, eqs 4a and 7a, which yields $[CrOF_4]^-$ as a transient species that dimerizes to form $[Cr_2O_2F_8]^{2-}$ in the solid state.

$$2XeF_6 + 2CrOF_4 \longrightarrow [XeF_5][Cr_2O_2F_8] + F_2 \qquad (7)$$

$$2[XeF_5][CrOF_5] \longrightarrow F_2 + \{2[XeF_5][CrOF_4]\} \longrightarrow [XeF_5]_2[Cr_2O_2F_8] \qquad (7a)$$

The X-ray structures of $[XeF_5]_2[Cr_2O_2F_8]$ (**3**), $[XeF_5]_2[Cr_2O_2F_8] \cdot 2HF$ (**4**), and $[XeF_5]_2[Cr_2O_2F_8] \cdot 2XeOF_4$ (**5**), show that the $[Cr_2O_2F_8]^{2-}$ anion is a fluorine-bridged dimer of $[CrOF_4]^-$ (see X-ray Crystallography).

$[XeF_5]_2[Cr_2O_2F_8] \cdot 2HF$ (4) and $[XeF_5]_2[Cr_2O_2F_8] \cdot 2XeOF_4$ (5). The reaction of equimolar amounts of XeF_6 and HF-wetted $CrOF_4$ in $CFCl_3$ solvent at room temperature yielded a mixture of $[XeF_5]_2[Cr_2O_2F_8] \cdot 2HF$ (**4**) and $[XeF_5]_2[Cr_2O_2F_8] \cdot 2XeOF_4$ (**5**), where compound (**4**) was the major component. Xenon hexafluoride was transferred onto a sample containing $CrOF_4$ and HF in $CFCl_3$ solvent at −196 °C. Upon warming to room temperature, $CrOF_4$ and XeF_6 rapidly dissolved to give a clear, amber-colored solution. Transparent, pale yellow-green, block-shaped crystals of $[XeF_5]_2[Cr_2O_2F_8] \cdot 2HF$ (**4**) and amber-colored crystals of $[XeF_5]_2[Cr_2O_2F_8] \cdot 2XeOF_4$ (**5**) slowly grew from solution when the sample was allowed to stand at −78 °C for 48 h.

An attempt to react equimolar amounts of XeF_6 and $CrOF_4$ in aHF at −78 °C only yielded crystalline $XeF_6 \cdot 1.5HF$ [24] and *α*-$CrOF_4$,[4] which were confirmed by unit cell

determinations. Upon warming to room temperature, $CrOF_4$ and XeF_6 rapidly dissolved in aHF to give an amber-colored solution. Quenching the sample at -196 °C yielded a white precipitate, which readily redissolved in aHF at room-temperature. Amber-colored, block-shaped crystals of $[XeF_5]_2[Cr_2O_2F_8]\cdot2XeOF_4$ (**5**) slowly grew from solution upon standing overnight at -78 °C.

The products resulting from the reactions of XeF_6 and $CrOF_4$ in aHF and in $CFCl_3$/aHF suggest that the reaction proceeds according to eq 7 and may be rationalized in terms of eqs 4a and 7a. The formation of $XeOF_4$ may be rationalized in terms of eqs 4a, 5a and 5b. Co-crystallized HF and $XeOF_4$ are likely introduced into the coordination spheres of $[XeF_5]^+$ and $[Cr_2O_2F_8]^{2-}$ upon crystallization from solution (see compounds (**4**) and (**5**) in X-ray Crystallography).


X-ray Crystallography

Details of data collection and crystallographic information pertaining to $[XeF_5]_2[CrF_6]\cdot2CrOF_4$ (**1**), $[Xe_2F_{11}]_2[CrF_6]$ (**2**), $[XeF_5]_2[Cr_2O_2F_8]$ (**3**), $[XeF_5]_2[Cr_2O_2F_8]\cdot2HF$ (**4**), $[XeF_5]_2[Cr_2O_2F_8]\cdot2XeOF_4$ (**5**), and $[XeF_5][Xe_2F_{11}][CrOF_5]\cdot2CrOF_4$ (**6**) are provided in Table 1.

The crystal structures contain $[XeF_5]^+$ and/or $[Xe_2F_{11}]^+$ cations which interact with their anions by means of Xe---F secondary bonds (fluorine bridges) (Tables S2–S6). In cases where the cations interact with more than one anion (compounds (**1**)–(**3**)), the formula units form columns by ion-pair formation between neighboring cations and anions (Figures 1–3 and S2–S4). The columns run parallel to the *b*-axis (**1** and **2**) and to the *c*-axis (**3**). The $[XeF_5]_2[Cr_2O_2F_8]$ ion-pairs of (**4**) are bridged through HF molecules, forming columns that run parallel to the *c*-axis and are well isolated from one another (Figure 4 and Figure S5). Additional Cr---F interactions occur between the $CrOF_4$ molecule and the fluorine atoms of

Table 1. Summary of X-ray Crystal Data and Refinement Results for $[XeF_5]_2[CrF_6]\cdot2CrOF_4$ (**1**), $[Xe_2F_{11}]_2[CrF_6]$ (**2**), $[XeF_5]_2[Cr_2O_2F_8]$ (**3**), $[XeF_5]_2[Cr_2O_2F_8]\cdot2HF$ (**4**), $[XeF_5]_2[Cr_2O_2F_8]\cdot2XeOF_4$ (**5**), and $[XeF_5][Xe_2F_{11}][CrOF_5]\cdot2CrOF_4$ (**6**)

Compound	1	2	3	4	5	6
space group	$P\bar{1}$	$C2/c$	$C2/c$	$P2_1/c$	$P\bar{1}$	$Pbca$
a (Å)	5.3743(3)	21.865(1)	16.4847(7)	10.7873(7)	7.435(1)	17.296(1)
b (Å)	9.3119(5)	5.5217(3)	9.1188(4)	9.1928(6)	8.750(1)	9.1078(5)
c (Å)	9.3636(5)	17.3532(8)	8.9770(4)	8.5616(5)	8.993(1)	27.694(2)
α (deg)	106.078(3)	90	90	90	90.920(2)	90
β (deg)	98.999(3)	115.191(3)	93.116(2)	106.870(2)	108.392(2)	90
γ (deg)	95.942(3)	90	90	90	97.838(2)	90
V (Å³)	439.37(4)	1895.9(2)	1347.4(1)	812.48(9)	548.9(1)	4362.6(4)
Z (molecules/unit cell)	1	4	4	4	1	16
mol. wt. (g mol^{-1})	906.60	1109.2	740.6	1641.28	1187.20	1148.90
calcd density (g cm^{-3})	3.441	3.886	3.651	3.354	3.591	3.500
T (°C)	−173	−173	−173	−173	−173	−173
μ (mm^{-1})	5.879	7.887	6.778	5.672	7.280	6.302
reflections collected	40698	20465	56817	106088	70190	58805
$R_1{}^a$	0.0375	0.0555	0.0282	0.0248	0.0305	0.0297
$wR_2{}^b$	0.0921	0.1071	0.059	0.0650	0.0754	0.0411

[a] R_1 is defined as $\Sigma||F_o| - |F_c||/\Sigma|F_o|$ for $I > 2\sigma\,(I)$. [b] wR_2 is defined as $[\Sigma[w(F_o{}^2)^2 - (F_c{}^2)^2]/\Sigma w(F_o{}^2)^2]^{\frac{1}{2}}$ for $I > 2\sigma(I)$.
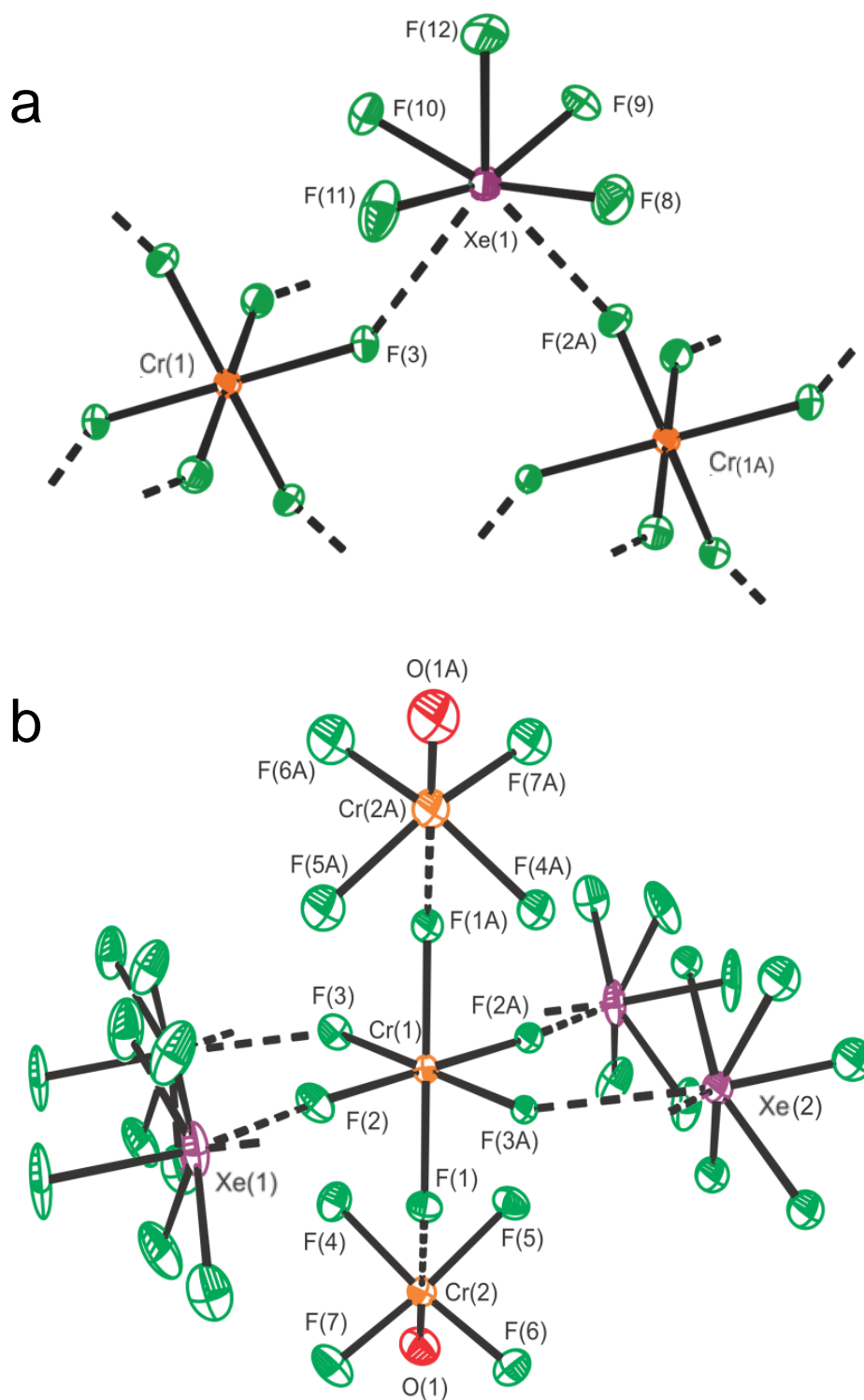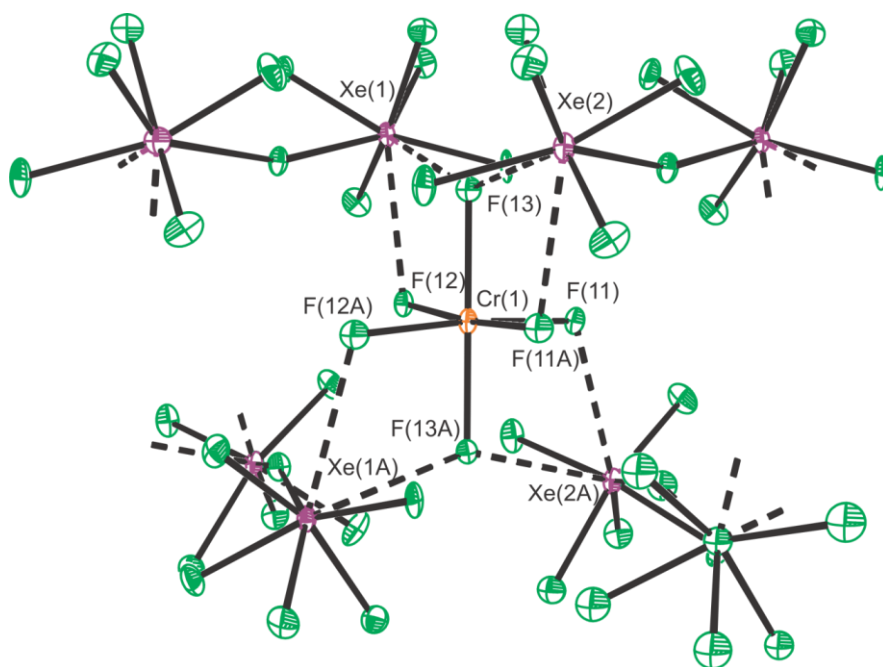
Figure 1. The X-ray crystal structure of $[XeF_5]_2[CrF_6]\cdot2CrOF_4$ (**1**) with thermal ellipsoids drawn at the 50% probability level. The coordination spheres of (a) the $[XeF_5]^+$ cation and (b) the $[CrF_6]^{2-}$ anion are depicted. Secondary Xe---F and Cr---F bonding interactions are indicated by dashed lines.
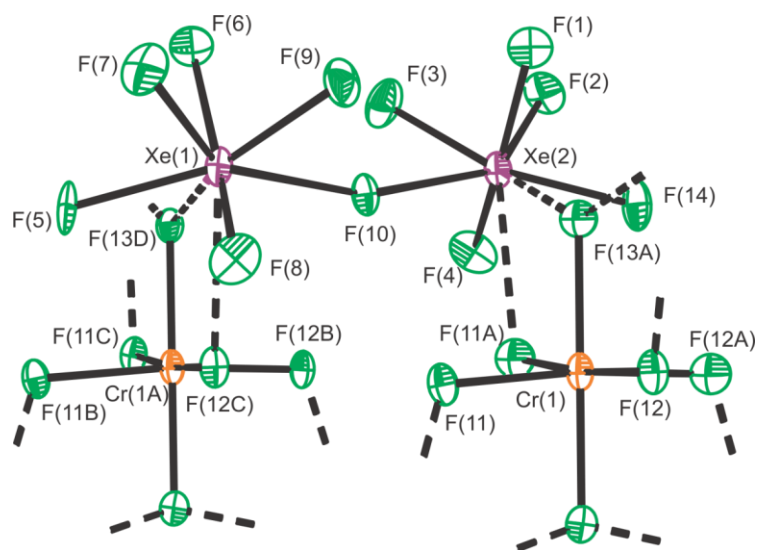
Figure 2. The X-ray crystal structure of [Xe$_2$F$_{11}$]$_2$[CrF$_6$] (**2**) with thermal ellipsoids drawn at the 50% probability level. The coordination spheres of (a) the [Xe$_2$F$_{11}$]$^+$ cation and (b) the [CrF$_6$]$^{2-}$ anion are depicted. Secondary Xe---F bonding interactions are indicated by dashed lines.

Figure 3. The X-ray crystal structure of $[XeF_5]_2[Cr_2O_2F_8]$ (**3**) with thermal ellipsoids drawn at the 50% probability level. The coordination spheres of (a) the $[XeF_5]^+$ cation and (b) the $[Cr_2O_2F_8]^{2-}$ anion are depicted. Secondary Xe---F bonding interactions are indicated by dashed lines.
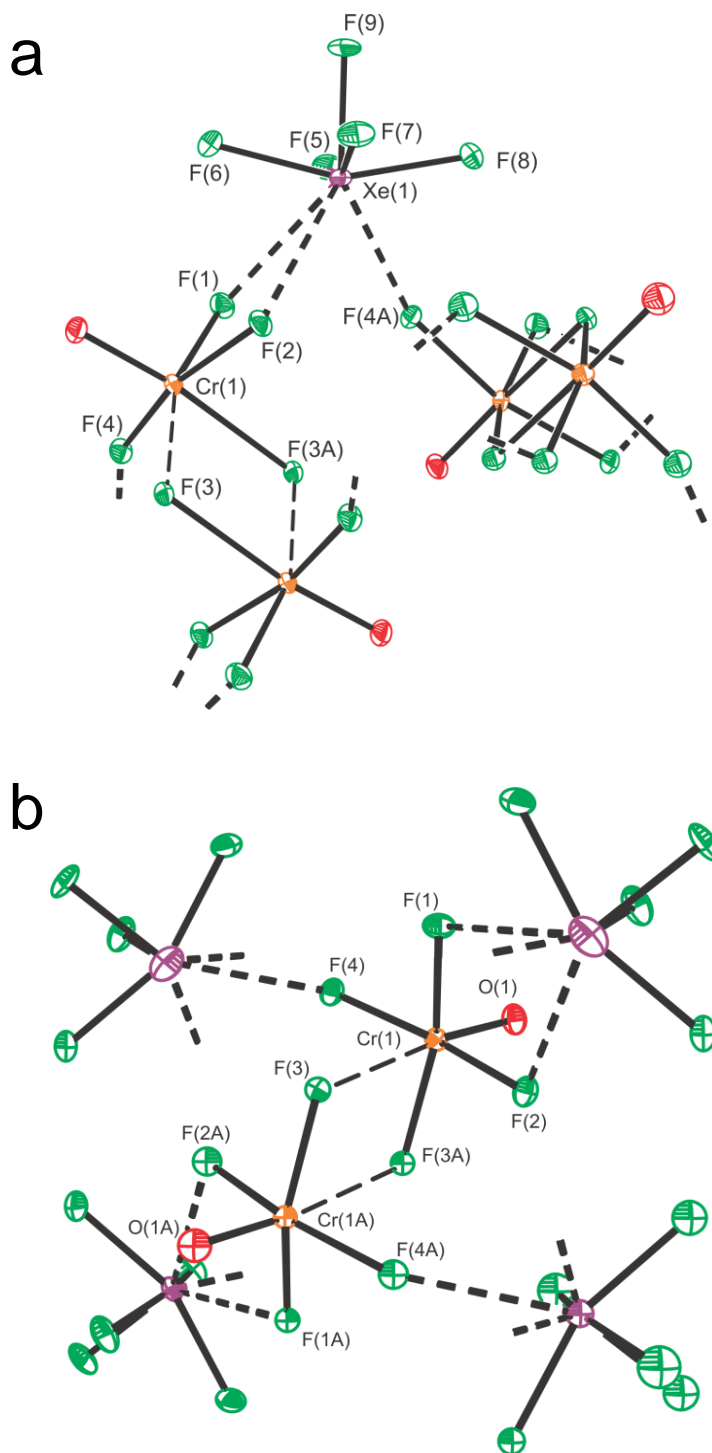
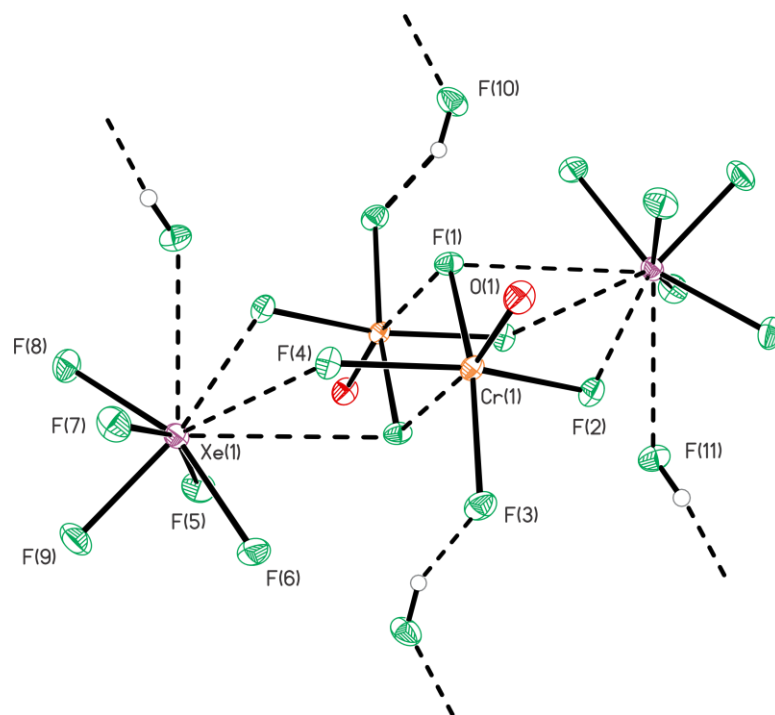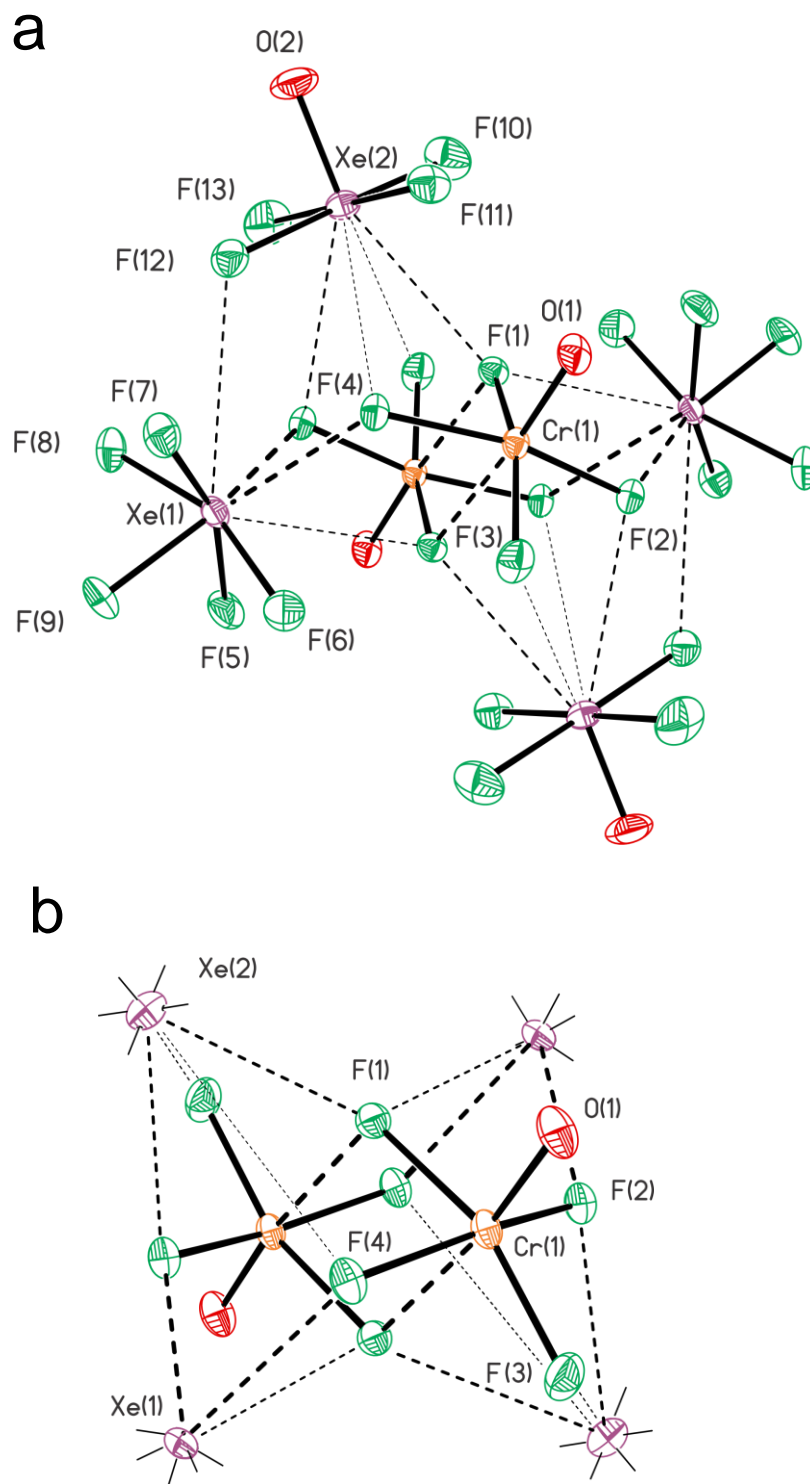**Figure 4.** The X-ray crystal structure of $[XeF_5]_2[Cr_2O_2F_8]\cdot 2HF$ (**4**) with thermal ellipsoids drawn at the 50% probability level. Secondary Xe---F bonding interactions are indicated by dashed lines.

their anions in $[XeF_5]_2[CrF_6]\cdot 2CrOF_4$ (**1**) and $[XeF_5][Xe_2F_{11}][CrOF_5]\cdot 2CrOF_4$ (**6**) (Figures 1 and 5, Tables S2 and S6). In contrast, $[XeF_5]_2[Cr_2O_2F_8]\cdot 2XeOF_4$ (**5**) and $[XeF_5][Xe_2F_{11}][CrOF_5]\cdot 2CrOF_4$ (**6**) do not form extended structures, but consist of well-isolated formula units having no significant intermolecular interactions with one another (Figures 5, 6, S6, and S7).

Structural units that are common to the aforementioned crystal structures are compared in separate sections in the ensuing discussion:

$[XeF_5]^+$ and $[Xe_2F_{11}]^+$. The bond lengths and bond angles of $[XeF_5]^+$ and $[Xe_2F_{11}]^+$ ($[\mu$-$F(XeF_5)_2]^+$) in all six salts and Xe---F contact distances (Tables S2−S6) are comparable to those observed in other $[XeF_5]^+$ and $[Xe_2F_{11}]^+$ salts, for example, $[Xe_2F_{11}][AuF_6]$,[23] $[XeF_5][OsO_3F_3]$,[21] $[XeF_5][OsO_3F_3]$,[21] and $[XeF_5][\mu$-$F(OsO_3F_2)_2]$.[21]

5

Figure 5. Depictions of (a) the X-ray crystal structure of $[XeF_5]_2[Cr_2O_2F_8]\cdot 2XeOF_4$ (**5**), and (b) the coordination environment around the $[Cr_2O_2F_8]^{2-}$ anion; thermal ellipsoids are drawn at the 50% probability level. Secondary Xe---F bonding interactions are indicated by dashed lines.
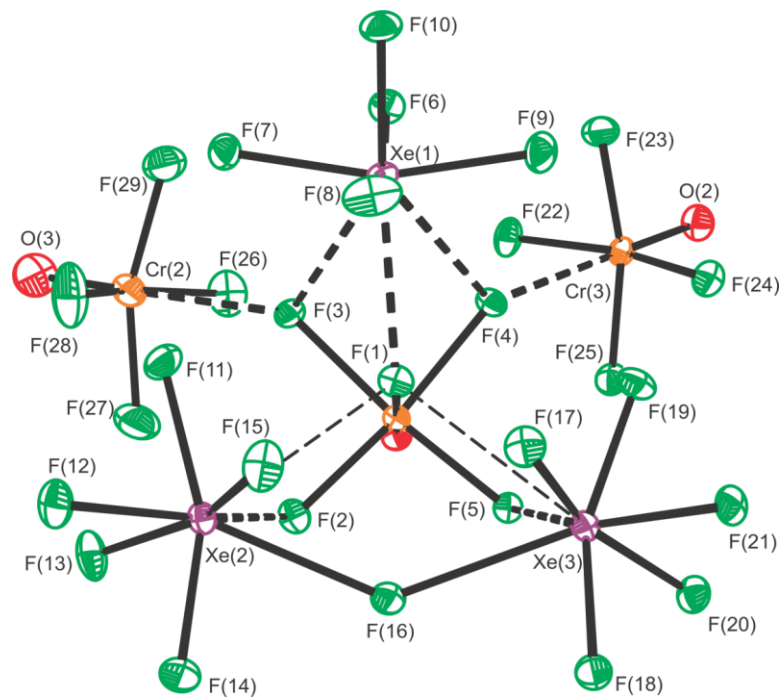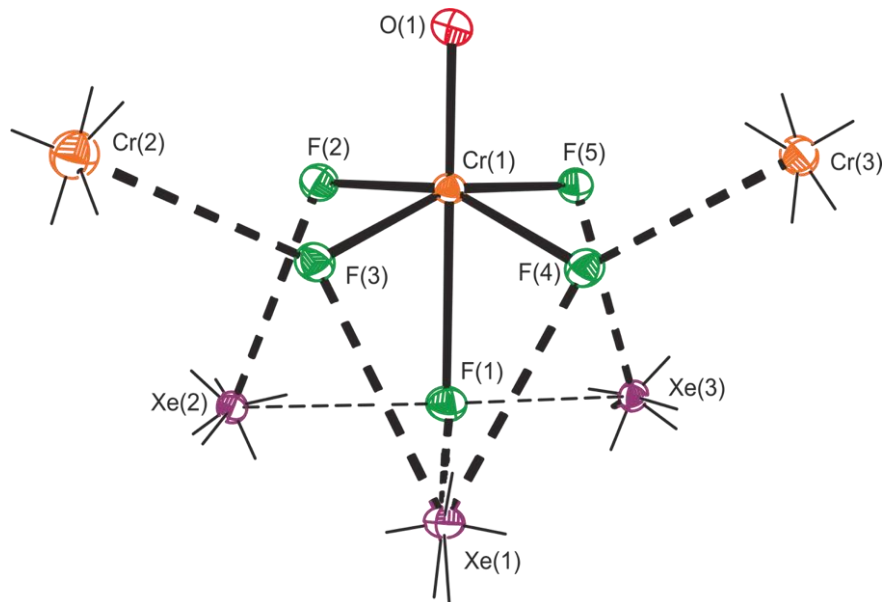
Figure 6. Depictions of (a) the asymmetric unit in the X-ray crystal structure of $[XeF_5][Xe_2F_{11}][CrOF_5]\cdot2CrOF_4$ (**6**) and (b) the environment around the $[CrOF_5]^{2-}$ anion; thermal ellipsoids are drawn at the 50% probability level. Secondary bonding interactions are indicated by dashed lines.

7

The $[XeF_5]^+$ cations may be described in terms of AX_5E VSEPR arrangements of five bond pairs (X) and a lone pair (E) which give rise to a square-pyramidal geometry.[25] The lone pair is located in the open square face of the square pyramid, and displaces the equatorial fluorine atoms towards the axial fluorine atom due to repulsions between the axial lone pair and $Xe-F_{eq}$ bond pairs. Consequently, negatively charged ligands that attempt to form contacts to the positively charged Xe atom must avoid the negatively charged $Xe-F_{eq}$ bond pairs and valence electron lone pair in the manner previously described by Bartlett *et al.* for $[XeF_5][RuF_6]$ [26] and $[XeF_5][PtF_6]$.[27] The $[XeF_5]^+$ cations in structures (**1**), and (**3**)–(**6**) interact with their respective anions through Xe---F secondary bonding interactions (Tables S2−S6) that are significantly less than the sum of the Xe and F van der Waals radii (3.61 Å).[28] Each $[XeF_5]^+$ cation in structure (**4**) also interacts with the fluorine atom of an HF molecule ($Xe---F_{(H)}$, 2.7985(9) Å), with a $Xe---F_{(H)}$ contact distance that is significantly shorter than those of $[XeF_5]_2[H_2F]\cdot HF$ ($Xe---F_{(H)}$, 3.006(5)–3.096(6)).[24] These secondary Xe---F contacts cap the triangular faces of the octahedra containing the valence electron lone pairs of Xe, resulting in Xe coordination numbers (excluding the stereoactive Xe lone pair) of 7, 8, and 9. A Xe coordination number of CN = 7 has been observed for $[Xe_2F_{11}][AuF_6]$,[23] whereas the most common Xe coordination numbers are CN = 8: e.g., $[XeF_5]_2[PdF_6]$,[29] $[XeF_5][AsF_6]$,[30] $[XeF_5][NiF_6]$,[31] and $[XeF_5][OsO_3F_3]$,[21] and CN = 9: e.g., $[XeF_5][SbF_6]\cdot XeOF_4$,[32] $[XeF_5][PtF_6]$,[27] $[XeF_5][AgF_4]$,[33] $[XeF_5][\mu-F(OsO_3F_2)_2]$,[21] $[Xe_2F_{11}][OsO_3F_3]$,[21] $[Xe_2F_{11}][AuF_6]$,[23] and $[Xe_2F_{11}][NiF_6]$.[34]

The Xe atoms (CN = 7) in $[XeF_5]_2[CrF_6]\cdot 2CrOF_4$ (**1**) (Figure 1), each have two contacts with two equatorial fluorine ligands of two $[CrF_6]^{2-}$ anions (Xe(1)---F(3), 2.435(8) Å; Xe(1)---F(2A), 2.435 Å). The Xe atom (CN = 8) of $[XeF_5]^+$ in $[XeF_5][Xe_2F_{11}][CrOF_5]\cdot 2CrOF_4$ (**6**) (Figure 4) has three contacts to the axial fluorine atom and equatorial fluorine atoms of the $[CrOF_5]^{2-}$

anion (Xe(1)---F(3), 2.624(2) Å; Xe(1)---F(4), 2.631(2) Å; Xe(1)---F(1), 2.461(2) Å). The Xe atoms (CN = 9) of $[XeF_5]_2[Cr_2O_2F_8]$ (**3**) (Figure 3) each have two Xe---F contacts with one $[Cr_2O_2F_8]^{2-}$ anion (Xe(1)---F(1), 2.6570(9) Å; Xe(1)---F(2), 2.6560 Å) and two Xe---F contacts with a second $[Cr_2O_2F_8]^{2-}$ anion (Xe(1)---F(4A), 2.4270(9) Å; Xe(1)---F(2A), 3.0229(9) Å). The Xe atoms are also nine-coordinate in $[XeF_5]_2[Cr_2O_2F_8]\cdot2HF$ (**4**) and $[XeF_5]_2[Cr_2O_2F_8]\cdot2XeOF_4$ (**5**), with each Xe having two shorter and one longer contact with a single $[Cr_2O_2F_8]^{2-}$ anion ((**4**): Xe(1)---F(2), 2.4581(8) Å; Xe(1)---F(4A), 2.4837(8) Å; Xe(1)---F(3), 3.0718(8) Å and (**5**): Xe(1)---F(2A), 2.518(1) Å; Xe(1)---F(4), 2.475(1) Å; Xe(1)---F(3), 3.039(1) Å) and one longer contact with a HF molecule ((**4**): Xe(1)---F(11), 2.7985(9) Å) or a F atom of a $XeOF_4$ molecule ((**5**): Xe(1)---F(12), 3.262(1) Å).

The $[Xe_2F_{11}]^+$ cations are comprised of two $[XeF_5]^+$ cations bridged by a fluoride ion. As in $[XeF_5]^+$, the F_{eq} atoms are displaced towards their respective F_{ax} atoms due to repulsions between their axial electron lone pairs and their Xe−F_{eq} bond pairs. The Xe atoms (CN = 8) of $[Xe_2F_{11}]_2[CrF_6]$ (**2**) (Figure 2) have contacts to one axial fluorine atom (Xe(1)---F13(D), 2.713(6) Å; (Xe(2)---F(13A), 2.711(6) Å) and one equatorial fluorine atom (Xe(1)---F(12C), 2.584(6) Å; Xe(2)---F(11A), 2.591(6) Å) of two different $[CrF_6]^{2-}$ anions. The Xe atoms (CN = 8) of $[Xe_2F_{11}]^+$ in $[XeF_5][Xe_2F_{11}][CrOF_5]\cdot2CrOF_4$ (**6**) have contacts to the axial fluorine ligand (Xe(2)---F(1), 2.824(2) Å; Xe(3)---F(1), 2.823(2) Å) and one equatorial fluorine ligand (Xe(2)---F(2), 2.661(2) Å; Xe(3)---F(5), 2.573(2) Å) of the same $[CrOF_5]^{2-}$ anion. Although the Xe---F cation-anion contact distances of both compounds are significantly shorter than the sum of the Xe and F van der Waals radii, they are significantly longer than the Xe---F_b bridge bonds of $[Xe_2F_{11}]^+$ ((**2**): Xe(1)−F(10), 2.247(6) Å and Xe(2)−F(10), 2.264(6) Å; (**6**): Xe(2)−F(16), 2.247(2) Å and Xe(3)−F(16), 2.332(2) Å). The Xe---F_b---Xe bridges of $[Xe_2F_{11}]^+$ are

9

asymmetric, differing by 0.017 and 0.085 Å for $[XeF_5][Xe_2F_{11}][CrOF_5]\cdot2CrOF_4$ (**6**) and $[Xe_2F_{11}]_2[CrF_6]$ (**2**), respectively.

XeOF₄. The bond lengths and bond angles around Xe are comparable to those of $XeOF_4\cdot XeF_2$.[35] As is the case for $[XeF_5]^+$ (*vide supra*) and $XeOF_4\cdot XeF_2$, the four Xe---F contacts to the Xe atom of $XeOF_4$ in $[XeF_5]_2[Cr_2O_2F_8]\cdot2XeOF_4$ (**5**) (2.968(1), 2.986(1), 3.337(1), 3.496(1) Å) occur in the open square face of the square-pyramidal $XeOF_4$ molecule, avoiding the valence electron lone pair that is trans to oxygen.

CrOF₄. The geometric parameters of the co-crystallized $CrOF_4$ molecules in $[XeF_5]_2[CrF_6]\cdot2CrOF_4$ (**1**) (Figure 1) and $[XeF_5][Xe_2F_{11}][CrOF_5]\cdot2CrOF_4$ (**6**) (Figure 6) are very similar to those of α- and β-$CrOF_4$ and $XeF_2\cdot2CrOF_4$ (Table 2).[4] The $CrOF_4$ molecules of both salts interact with the fluorine ligands of their respective anions through Cr---F contacts that are trans to their Cr=O bonds. The $CrOF_4$ molecules of $[XeF_5][Xe_2F_{11}][CrOF_5]\cdot2CrOF_4$ interact with two adjacent equatorial fluorine ligands of the $[CrOF_5]^{2-}$ anion (Cr(2)---F(3), 2.486(2) Å; Cr(3)---F(4), 2.393(2) Å). The $CrOF_4$ molecules of $[XeF_5]_2[CrF_6]\cdot2CrOF_4$ (**1**) are trans to one another, interacting with the axial fluorine ligands of the $[CrF_6]^{2-}$ anion (Cr(2)---F(1), 2.215(3) Å). These contacts are shorter than those in α-$CrOF_4$ (2.274(3)–2.333(3) Å), β-$CrOF_4$ (2.3659(6) Å) and $XeF_2\cdot2CrOF_4$ (Cr(2)---F(1), 2.386(1) Å). The Cr−O bonds of $[XeF_5]_2[CrF_6]\cdot2CrOF_4$ (**1**) (1.565(6) Å) and $[XeF_5][Xe_2F_{11}][CrOF_5]\cdot2CrOF_4$ (**6**) (1.526(3) Å and 1.545(3) Å) have significant double bond character and are comparable in length to those of α-$CrOF_4$ (1.539(3)–1.558(4) Å), β-$CrOF_4$ (1.5490(7) Å)[4] and $XeF_2\cdot2CrOF_4$ (1.545(2) Å).[4] As expected, the fluorine ligands are bent away from the sterically more demanding Cr−O double bond domains of the $CrOF_4$ molecules in accordance with the VSEPR model of molecular geometry.[25]

Table 2. Experimental Geometric Parameters for the $[CrF_6]^{2-}$ Anion in $[XeF_5]_2[CrF_6] \cdot 2CrOF_4$ (**1**)

Bond Lengths (Å)			
Cr(1)−F(1)	1.817(6)	Cr(1)−F(3)	1.818(7)
Cr(1)−F(2)	1.808(6)		
Bond Angles (deg)			
F(1)−Cr(1)−F(2)	90.0(3)	F(2)−Cr(1)−F(1A)	90.0(3)
F(1)−Cr(1)−F(3)	89.7(3)	F(3)−Cr(1)−F(2A)	89.7(2)
F(1)−Cr(1)−F(2A)	90.1(3)	F(3)−Cr(1)−F(3A)	180.0(2)
F(1)−Cr(1)−F(3A)	90.3(3)	F(3)−Cr(1)−F(1A)	90.3(3)
F(1)−Cr(1)−F(1A)	180.0(3)	F(2A)−Cr(1)−F(3A)	89.2(3)
F(2)−Cr(1)−F(3)	89.0(3)	F(2A)−Cr(1)−F(1A)	89.9(3)
F(2)−Cr(1)−F(2A)	180.0(3)	F(3A)−Cr(1)−F(1A)	89.7(3)
F(2)−Cr(1)−F(3A)	91.0(3)		

Table 3. Experimental Geometric Parameters for the $[CrF_6]^{2-}$ Anion in $[Xe_2F_{11}]_2[CrF_6]$ (**2**)

Bond Lengths (Å)			
Cr(1)−F(11)	1.796(6)	Cr(1)−F(13)	1.854(6)
Cr(1)−F(12)	1.800(6)		
Bond Angles (deg)			
F(11)−Cr(1)−F(12)	90.17(3)	F(12)−Cr(1)−F(13A)	87.20(3)
F(11)−Cr(1)−F(13)	92.95(3)	F(13)−Cr(1)−F(11A)	87.32(3)
F(11)−Cr(1)−F(11A)	180.0(3)	F(13)−Cr(1)−F(12A)	92.54(3)
F(11)−Cr(1)−F(12A)	174.51(3)	F(13)−Cr(1)−F(13A)	180.0(4)
F(11)−Cr(1)−F(13A)	87.20(3)	F(11A)−Cr(1)−F(12A)	90.54(3)
F(12)−Cr(1)−F(13)	87.20(3)	F(11A)−Cr(1)−F(13A)	92.54(4)
F(12)−Cr(1)−F(11A)	90.54(3)	F(12A)−Cr(1)−F(13A)	87.32(3)
F(12)−Cr(1)−F(12A)	180.0(3)		

[CrF₆]²⁻. The Cr–F bonds of the $[CrF_6]^{2-}$ anion in $[XeF_5]_2[CrF_6]\cdot 2CrOF_4$ (**1**) (Figure 1) are nearly equal, resulting in a Cr atom coordination sphere that is close to octahedral (Table 2). The four equatorial Cr–F$_{eq}$ bonds of $[CrF_6]^{2-}$ in $[Xe_2F_{11}]_2[CrF_6]$ (**2**) (Figure 2) are equal within ±3σ (Cr(1)–F(11), 1.796(6) Å; Cr(1)–F(12) 1.800(6) Å), and are significantly shorter than the terminal Cr–F$_{ax}$ bonds (Cr(1)–F(13), 1.854(6) Å), resulting in a local Cr environment that is close to D_{4h} symmetry (Table 3). The Cr–F$_{eq}$ bond lengths of $[Xe_2F_{11}]_2[CrF_6]$ (**2**) are equal, within ±3σ, to those of $[XeF_5]_2[CrF_6]\cdot 2CrOF_4$ (**1**). The longer Cr–F$_{ax}$ bonds of $[Xe_2F_{11}]_2[CrF_6]$ (**2**) are a consequence of the intermolecular contacts between the F$_{ax}$ ligands and the Xe atoms of two different $[Xe_2F_{11}]^+$ cations (F(13)---Xe(1), 2.708(6), F(13)---Xe(2), 2.716(6) Å). The Cr–F bond lengths of both $[CrF_6]^{2-}$ anions are comparable to those of Li₂CrF₆ (4 x 1.829(3), 2 x 1.812(4) Å),[36] and are intermediate with respect to the terminal and bridging Cr–F bonds of the known chromium fluoride species in which Cr(IV) is coordinated to six fluorine ligands, namely XeF₂·CrF₄ (Cr–F$_t$, 1.683(3)–1.750(2) Å; Cr–F$_b$, 1.839(2)–2.099(2) Å) and [XeF₅][CrF₅] (Cr–F$_t$, 1.675(11)–1.825(10) Å; Cr–F$_b$, 1.900(9)–1.971(10) Å).[22]

[Cr₂O₂F₈]²⁻. The $[Cr_2O_2F_8]^{2-}$ anion (Figures 3–5, Tables 4 and 5) can be described in terms of two symmetry-equivalent $[CrOF_4]^-$ anions which share a fluorine bridge atom (F(3) and F(3A)). As expected, the Cr–F$_b$ bridge bonds (2.1177(9) (**3**), 2.2237(8) (**4**), 2.265(1) (**5**) Å) are significantly longer than the equatorial Cr–F$_{eq}$ bonds, which range from 1.7939(9) to 1.8516(9) (**3**), 1,7940(8) to 1.8739(7) (**4**), and 1.733(1) to 1.904(1) (**5**) Å. The shortest Cr–F$_{eq}$ bond length observed in (**5**) (1.733(1) Å) corresponds to the only F$_{eq}$ that is free of secondary bonding interactions (Table S5) and is comparable to the terminal Cr–F$_{eq}$ bonds observed in α-CrOF₄ (1.707(2)–1.729(2) Å) and β-CrOF₄ (1.7212(6)–1.7372(6) Å).[4] The Cr–O bond lengths (1.567(1) (**3**), 1.5438(9) (**4**), 1.549(1) (**5**) Å) are characteristic of Cr–O double bonds, and are slightly longer than those of Cr^{V}OF₃ (1.542(5) Å),[16] α-Cr^{VI}OF₄ (1.539(3)–1.558(4) Å),

Table 4. Experimental Geometric Parameters for [XeF$_5$]$_2$[Cr$_2$O$_2$F$_8$] **(3)** and [XeF$_5$]$_2$[Cr$_2$O$_2$F$_8$]·2HF **(4)**

	(3)	(4)		(3)	(4)
		Bond Lengths and Contacts (Å)			
Cr(1)−O(1)	1.567(1)	1.5438(9)	Cr(1)−F(3A)	1.8515(9)	1.8730(7)
Cr(1)−F(1)	1.7939(9)	1.7940(8)	Cr(1)−F(4)	1.8326(9)	1.8362(8)
Cr(1)−F(2)	1.8497(9)	1.8398(8)	Cr(1)---F(3)	2.1177(9)	2.2237(8)
		Bond Angles (deg)			
O(1)−Cr(1)−F(1)	102.53(6)	103.20(5)	O(1)−Cr(1)−F(4)	97.12(5)	99.55(5)
O(1)−Cr(1)−F(2)	97.00(5)	97.32(4)	O(1)−Cr(1)---F(3)	171.35(5)	169.75(4)
O(1)−Cr(1)−F(3A)	98.28(5)	98.85(4)	F(1)−Cr(1)−F(4)	89.08(4)	88.28(4)
F(1)−Cr(1)−F(2)	85.16(4)	89.37(4)	F(1)−Cr(1)---F(3)	86.09(4)	86.15(3)
F(1)−Cr(1)−F(3A)	159.09(4)	157.85(4)	F(2)−Cr(1)−F(4)	165.61(4)	163.06(4)
F(2)−Cr(1)−F(3A)	90.35(4)	89.89(4)	F(2)−Cr(1)---F(3)	84.39(4)	78.36(3)
F(3A)−Cr(1)−F(4)	90.36(4)	86.02(4)	F(4)−Cr(1)---F(3)	82.07(4)	84.75(3)
F(3A)−Cr(1)---F(3)	73.14(4)	72.03(3)	Cr(1)---F(3)−Cr(1A)	106.86(4)	107.97(3)

Table 5. Experimental and Calculated Geometric Parameters for [XeF$_5$]$_2$[Cr$_2$O$_2$F$_8$]·2XeOF$_4$ **(5)** and [Cr$_2$O$_2$F$_8$]$^{2-}$ **(5')**

	exptl	calcd[a]			exptl	calcd[a]	
	(5)	(5)	(5')		(5)	(5)	(5')
			Bond Lengths and Contacts (Å)				
Cr(1)−O(1)	1.549(1)	1.487	1.523	Cr(1)−F(3)	1.733(1)	1.722	1.784
Cr(1)−F(1)	1.904(1)	1.832	1.819	Cr(1)−F(4)	1.840(1)	1.833	1.767
Cr(1)−F(2)	1.854(1)	1.857	1.767	Cr(1)---F(1A)	2.265(1)	2.335	2.432
			Bond Angles (deg)				
O(1)−Cr(1)−F(1)	100.92(6)	105.03	100.93	O(1)−Cr(1)−F(4)	99.17(6)	100.57	102.66
O(1)−Cr(1)−F(2)	98.92(6)	101.05	102.12	O(1)−Cr(1)---F(1A)	172.40(6)	176.78	171.7
O(1)−Cr(1)−F(3)	105.63(7)	106.69	102.66	F(1)−Cr(1)−F(4)	87.20(5)	87.04	88.13
F(1)−Cr(1)−F(2)	84.17(4)	84.58	88.14	F(1)−Cr(1)---F(1A)	71.63(5)	71.75	70.77
F(1)−Cr(1)−F(3)	153.22(5)	148.13	156.41	F(2)−Cr(1)−F(4)	161.13(4)	158.19	155.75
F(2)−Cr(1)−F(3)	88.24(5)	86.46	86.95	F(2)−Cr(1)---F(1A)	82.05(4)	78.95	78.08
F(3)−Cr(1)−F(4)	92.01(5)	90.15	86.94	F(4)−Cr(1)---F(1A)	79.31(4)	79.31	78.06
F(3)−Cr(1)---F(1A)	81.91(5)	76.53	85.64	Cr(1)---F(1)−Cr(1A)	108.37(5)	108.25	109.22

[a] The PBE1PBE/aug-cc-pVDZ(Xe)-Def2-SVP (F, O, Cr) level of theory was used.

and β-Cr^{VI}OF$_4$ (1.5490(7) Å).[4] The four equatorial fluorine ligands are bent away from the Cr−O double bond domain, and the F$_b$---Cr−F$_b$ angles (73.14(4) (**3**), 72.03(3) (**4**), 71.63(4) (**5**)°) are significantly smaller than the F$_{eq}$−Cr---F$_b$ angles (82.07(4)−86.09(4) (**3**), 78.36(3)−86.15(3) (**4**), 79.31(4)−82.05(4) (**5**)°).

[CrOF$_5$]$^{2-}$. The primary chromium coordination sphere of [CrOF$_5$]$^{2-}$ (Figure 6, Table 6) in [XeF$_5$][Xe$_2$F$_{11}$][CrOF$_5$]·2CrOF$_4$ (**6**) consists of four equatorial fluorine ligands and an axial fluorine ligand trans to the oxygen ligand. The Cr−F$_{ax}$ bond length (2.120(2) Å) is significantly longer than the Cr−F$_{eq}$ bond lengths (1.813(2)−1.876(2) Å). The elongation is attributed to the *trans*-effect of oxygen and to three Xe---F$_{ax}$ contacts (Xe(1)---F(1), 2.461(2), Xe(2)---F(1), 2.823(2), Xe(3)---F(1), 2.824(2) Å) to the Xe atoms of the neighboring cations (*vide supra*). The equatorial fluorine ligands of [CrOF$_5$]$^{2-}$ interact with [XeF$_5$]$^+$, [Xe$_2$F$_{11}$]$^+$, and CrOF$_4$ through a number of Xe---F$_{eq}$ and Cr---F$_{eq}$ contacts, which account for the wide range of observed Cr−F$_{eq}$ bond lengths (1.813(2)–1.875(2) Å). The shorter distances correspond to single contacts with the [Xe$_2$F$_{11}$]$^+$ cation, whereas the longer distances correspond to contacts with the [XeF$_5$]$^+$ and [Xe$_2$F$_{11}$]$^+$ cations and two Cr---F$_{eq}$ contacts with the two CrOF$_4$ molecules. The Cr−O bond length of [CrOF$_5$]$^{2-}$ (1.545(3) Å) is comparable to those of CrOF$_3$ (1.542(5) Å),[16] α-CrOF$_4$ (1.539(3)−1.558(4) Å), and β-CrOF$_4$ (1.5490(7) Å).[4]

Raman Spectroscopy

The low-temperature Raman spectra of [XeF$_5$]$_2$[Cr$_2$O$_2$F$_8$]·2XeOF$_4$ (**5**) and [XeF$_5$]Xe$_2$F$_{11}$][CrOF$_5$]·2CrOF$_4$ (**6**) are shown in Figures 7a and 7b. The Raman spectra were collected on crystalline samples which were shown to be compounds (**5**) and (**6**) by single-crystal X-ray structure determinations (see X-ray Crystallography). Spectral assignments were made by comparison with the calculated vibrational frequencies and intensities of the energy-minimized, gas-phase geometries of [XeF$_5$]$_2$[Cr$_2$O$_2$F$_8$]·2XeOF$_4$ (**5**) and

Table 6. Experimental and Calculated Geometric Parameters of [XeF$_5$][Xe$_2$F$_{11}$][CrOF$_5$]·2CrOF$_4$ **(6)** and [CrOF$_5$]$_2$$^-$ **(6')**

	exptl	calcd			exptl	calcd	
			Bond Lengths (Å)				
	(6)	**(6)**	**(6')**		**(6)**	**(6)**	**(6')**
Cr(1)−O(1)	1.545(3)	1.491	1.559	Cr(1)−F(3)	1.869(2)	1.836	1.883
Cr(1)−F(1)	2.120(2)	2.233	1.889	Cr(1)−F(4)	1.875(2)	1.825	1.883
Cr(1)−F(2)	1.813(2)	1.807	1.883	Cr(1)−F(5)	1.823(2)	1.814	1.883
			Bond Angles (deg)				
O1−Cr1−F1	176.87(11)	178.12	180.0	F1−Cr1−F5	81.46(8)	79.98	85.75
O1−Cr1−F2	100.65(11)	102.51	94.25	F2−Cr1−F3	89.12(9)	88.86	89.69
O1−Cr1−F3	98.64(10)	102.27	94.25	F2−Cr1−F4	159.69(8)	153.37	171.51
O1−Cr1−F4	99.09(10)	103.98	94.25	F2−Cr1−F5	90.88(9)	88.59	89.69
O1−Cr1−F5	100.61(10)	101.89	94.25	F3−Cr1−F4	83.22(8)	83.00	89.69
F1−Cr1−F2	81.60(8)	77.64	85.75	F3−Cr1−F5	160.41(8)	155.69	171.51
F1−Cr1−F3	79.16(8)	75.85	85.75	F4−Cr1−F5	90.17(8)	88.57	89.69
F1−Cr1−F4	78.50(8)	75.79	85.75				

[a] The PBE1PBE/aug-ccpVDZ(Xe)-Def2-SVP (F, O, Cr) level of theory was used.
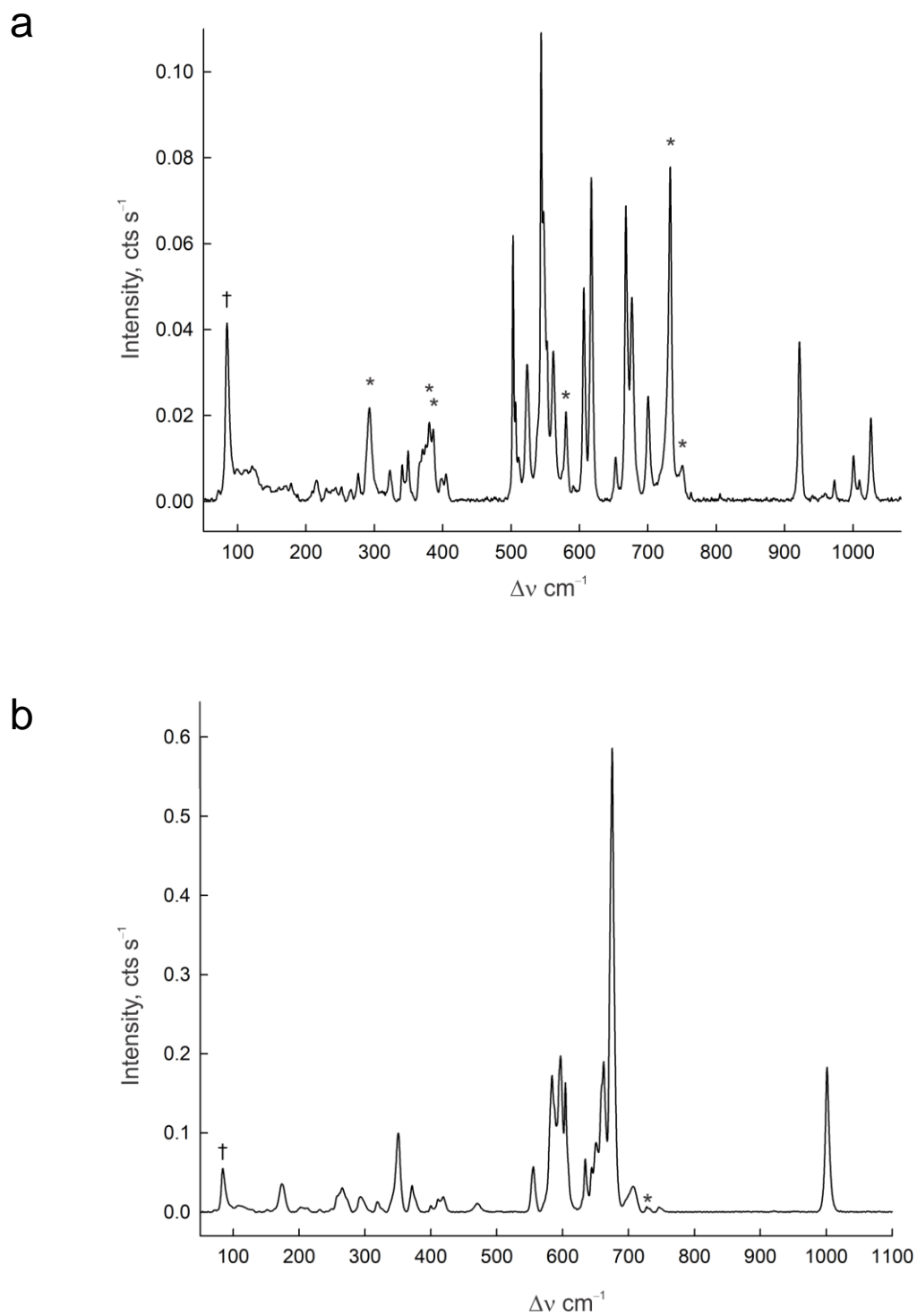
Figure 7. Raman spectra of (a) $[XeF_5]_2[Cr_2O_2F_8] \cdot 2XeOF_4$ (**5**) and (b) $[XeF_5][Xe_2F_{11}][CrOF_5]$ $\cdot 2CrOF_4$ (**6**) recorded at $-140\ ^oC$ using 1064-nm excitation. The symbol (†) denotes an instrumental artifact. The symbol (*) denotes bands attributable to FEP.

16

[XeF$_5$]Xe$_2$F$_{11}$][CrOF$_5$]·2CrOF$_4$ (**6**) at the PBE1PBE/aug-cc-pVDZ-Def2SVP level of theory. Vibrational assignments for CrOF$_4$, XeOF$_4$, and the [XeF$_5$]$^+$ and [Xe$_2$F$_{11}$]$^+$ cations were also aided by comparison with polymeric CrOF$_4$,[4] XeOF$_4$·XeF$_2$,[36] [XeF$_5$][OsO$_3$F$_3$],[21] [XeF$_5$][AsF$_6$],[30] [XeF$_5$][BF$_4$],[37] [Xe$_2$F$_{11}$][AuF$_6$],[23] [Xe$_2$F$_{11}$][PdF$_6$],[23] and [Xe$_2$F$_{11}$][OsO$_3$F$_3$].[21] The observed and calculated frequencies, their detailed assignments, and mode descriptions are provided in Tables S7 and S8. With the exception of the overestimated v(Cr-O) and underestimated v(Xe-O) stretching frequencies, the experimental vibrational frequencies and their trends are well reproduced by the calculated frequencies.

[XeF$_5$]$_2$[Cr$_2$O$_2$F$_8$]·2XeOF$_4$ (5). Several bands are split in the Raman spectrum of [XeF$_5$]$_2$[Cr$_2$O$_2$F$_8$]·2XeOF$_4$ (Table S7). To account for these splittings, a factor-group analysis based on the X-ray crystal structure of (**5**) (Figure S9) was carried out using the "correlation method".[38] A total of 102 vibrational modes are predicted for gas-phase [XeF$_5$]$_2$[Cr$_2$O$_2$F$_8$]·2XeOF$_4$ under C_i symmetry. The vibrations belong to the irreducible representations Γ = 51A$_g$ + 51A$_u$, where the A$_g$ and A$_u$ modes are Raman- and infrared-active, respectively. The A$_g$ and A$_u$ representations of gas-phase [XeF$_5$]$_2$[Cr$_2$O$_2$F$_8$]·2XeOF$_4$ (**5**) under C_i symmetry correlate to A irreducible representations under C_1 site symmetry in the solid state and to A representations under the unit cell symmetry (C_1). Consequently, all 102 modes are rendered both Raman and infrared active (Figure S9) under the unit cell symmetry.

The band observed at 1026 cm^{-1} is assigned to the symmetric v(Cr-O) stretch and occurs at higher frequency than in Cr^{V}OF$_3$ (Ra) (1000 cm^{-1})[15] and Cs[Cr^{V}OF$_4$] (IR) (1005 cm^{-1}) (Figure 7).[18] The calculated frequency for v(Cr-O) increases upon ion-pair formation (anion: 1176 cm^{-1}; ion-pair: 1266 cm^{-1}). The diversity of Cr–F bonds results in v(Cr-F) stretching modes that range from 398 to 700 cm^{-1} (calcd: 369–729 cm^{-1}) (Table S7). The band at 398 cm^{-1} involves the bridging F atoms and corresponds to [v(Cr$_1$-F$_1$) + v(Cr$_1$-F$_{1A}$)] + [v(Cr$_{1A}$-F$_1$) + v(Cr$_{1A}$-F$_{1A}$)]; however, the out-of-phase counterpart, [v(Cr$_1$-F$_1$) + v(Cr$_1$-F$_{1A}$)] − [v(Cr$_{1A}$-F$_1$) +

v(Cr$_{1A}$-F$_{1A}$)], was not observed but it is expected to be weak and is predicted to occur at much lower frequency (225 cm^{-1}). The bands at 370 and 375 cm^{-1} are assigned to δ(FCrO) deformation modes (calcd: 359, 364 cm^{-1}) by comparison with analogous modes in CrOF$_4$.[4]

[XeF$_5$]Xe$_2$F$_{11}$][CrOF$_5$]·2CrOF$_4$ (6). The medium intensity band at 1000 cm^{-1} (Table S8) is assigned to the overlapping Cr−O stretches of CrOF$_4$ (calcd: 1230, 1232 cm^{-1}) and [CrOF$_5$]$^{2-}$ (calcd: 1230, 1193 cm^{-1}), consistent with the very similar Cr−O bond lengths of CrOF$_4$ (1.526(3) and 1.545(3) Å) and [CrOF$_5$]$^{2-}$ (1.545(3) Å) in the crystal structure of (**6**). The calculated v(Cr-O) frequency of [CrOF$_5$]$^{2-}$ increases significantly upon ion-pair formation (anion: 1009 cm^{-1}; ion-pair: 1193 cm^{-1}). The bands between 700 and 750 cm^{-1} (calcd: 722−762 cm^{-1}) are assigned to Cr-F stretching modes of the coordinated CrOF$_4$ molecules and do not couple to any of the cation or anion modes. Similar modes associated with the [CrOF$_5$]$^{2-}$ anion occur at lower frequencies, which are consistent with longer Cr−F bonds in the anion (1.813(2)–1.875(2) Å) than in the coordinated CrOF$_4$ molecules (1.734(2)–1.745(2) Å) of (**6**). The latter stretching modes are coupled to Xe-F stretching modes of the cations. The bands observed between 555 and 608 cm^{-1} (calcd: 562−602 cm^{-1}) are comprised of Cr-F stretches from both [CrOF$_5$]$^{2-}$ and CrOF$_4$ that are coupled to Xe-F stretches of both [XeF$_5$]$^+$ and [Xe$_2$F$_{11}$]$^+$. The band at 470 cm^{-1} (calcd: 469 cm^{-1}) results from coupling of the Cr-F$_e$ stretches of [CrOF$_5$]$^{2-}$ to the Xe-F$_e$ stretches of [Xe$_2$F$_{11}$]$^+$. The bands between 372 and 419 cm^{-1} are mainly assigned to δ(FCrO) and to δ(FCrF) deformation modes (calcd: 357−413 cm^{-1}) from both [CrOF$_5$]$^{2-}$ and CrOF$_4$. The umbrella modes, δ$_{umb}$(CrF$_{4e}$), of CrOF$_4$ occur at lower frequencies (exptl: 343, 351 cm^{-1}; calcd: 344−354 cm^{-1}) and are coupled to δ(FXeF) deformation modes of [XeF$_5$]$^+$ and [Xe$_2$F$_{11}$]$^+$.

COMPUTATIONAL RESULTS

Calculated Geometries

The geometry-optimized gas-phase structures of $[XeF_5]_2[Cr_2O_2F_8]\cdot2XeOF_4$, $[Cr_2O_2F_8]^{2-}$, $[XeF_5][Xe_2F_{11}][CrOF_5]\cdot2CrOF_4$, and $[CrOF_5]^{2-}$ were optimized at the PBE1PBE/aug-cc-pVDZ(Xe)-Def2-SVP (F, O, Cr) level of theory and resulted in stationary points with all frequencies real (Tables S7–S10). The starting geometries used for $[XeF_5]_2[Cr_2O_2F_8]\cdot2XeOF_4$, $[Cr_2O_2F_8]^{2-}$, $[XeF_5][Xe_2F_{11}][CrOF_5]\cdot2CrOF_4$, and $[CrOF_5]^{2-}$ were the crystallographic geometries obtained from their respective salts. All trends observed in thecrystal structures are reproduced by the calculated geometries of (**5**) and (**6**), including the secondary bond lengths and their associated contact angles. The greatest discrepancies occur for the Cr−O and Cr−F bond lengths, which are underestimated, and the Xe−F bond lengths, which are overestimated.

[XeF₅]₂[Cr₂O₂F₈]·2XeOF₄ (C₁) and [Cr₂O₂F₈]²⁻ (C₂ₕ). The $[Cr_2O_2F_8]^{2-}$ anion optimized to C_{2h} symmetry (Figure 8). The Cr−F$_t$ bond that is trans to the Cr-F$_b$ bridge bond is slightly shorter (1.767 Å) than the Cr−F$_t$ bonds (1.784 Å) that are cis to the Cr–F$_b$ bridge bond (1.819 Å). As expected, the Cr−F$_t$ bonds are significantly shorter than the Cr---F$_b$ contact distances (2.432 Å). Upon salt formation, the Cr−F$_b$ and Cr---F$_b$ bonds in $[XeF_5]_2[Cr_2O_2F_8]\cdot2XeOF_4$ (1.832 and 2.335 Å) changed very little (Figure 8). Three of the terminal Cr−F$_t$ bonds elongate due to Xe---F contacts with $XeOF_4$ and $[XeF_5]^+$, whereas the Cr−F$_t$ bond, with no significant contacts, and the Cr–O bond are significantly shorter (1.722 and 1.487 Å, respectively) than in the isolated anion (1.784 and 1.523 Å). Bond length contraction is therefore only observed for bonds that do not have significant secondary bonding interactions, and is likely due to increased polarization of the Cr–F$_t$ and Cr−O bonds that are trans to terminal fluorine ligands that have short contacts to neighboring Xe or Cr atoms.
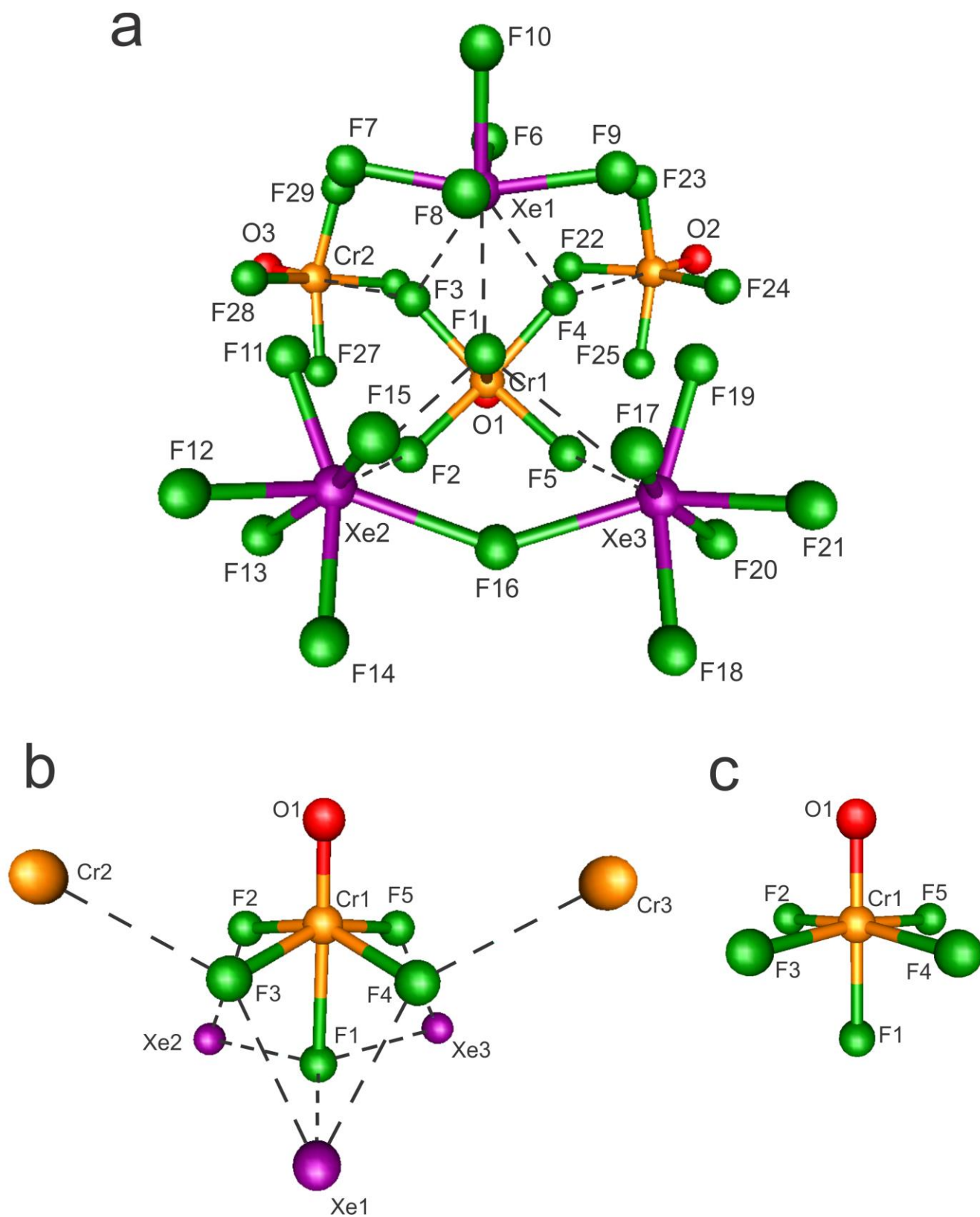
19
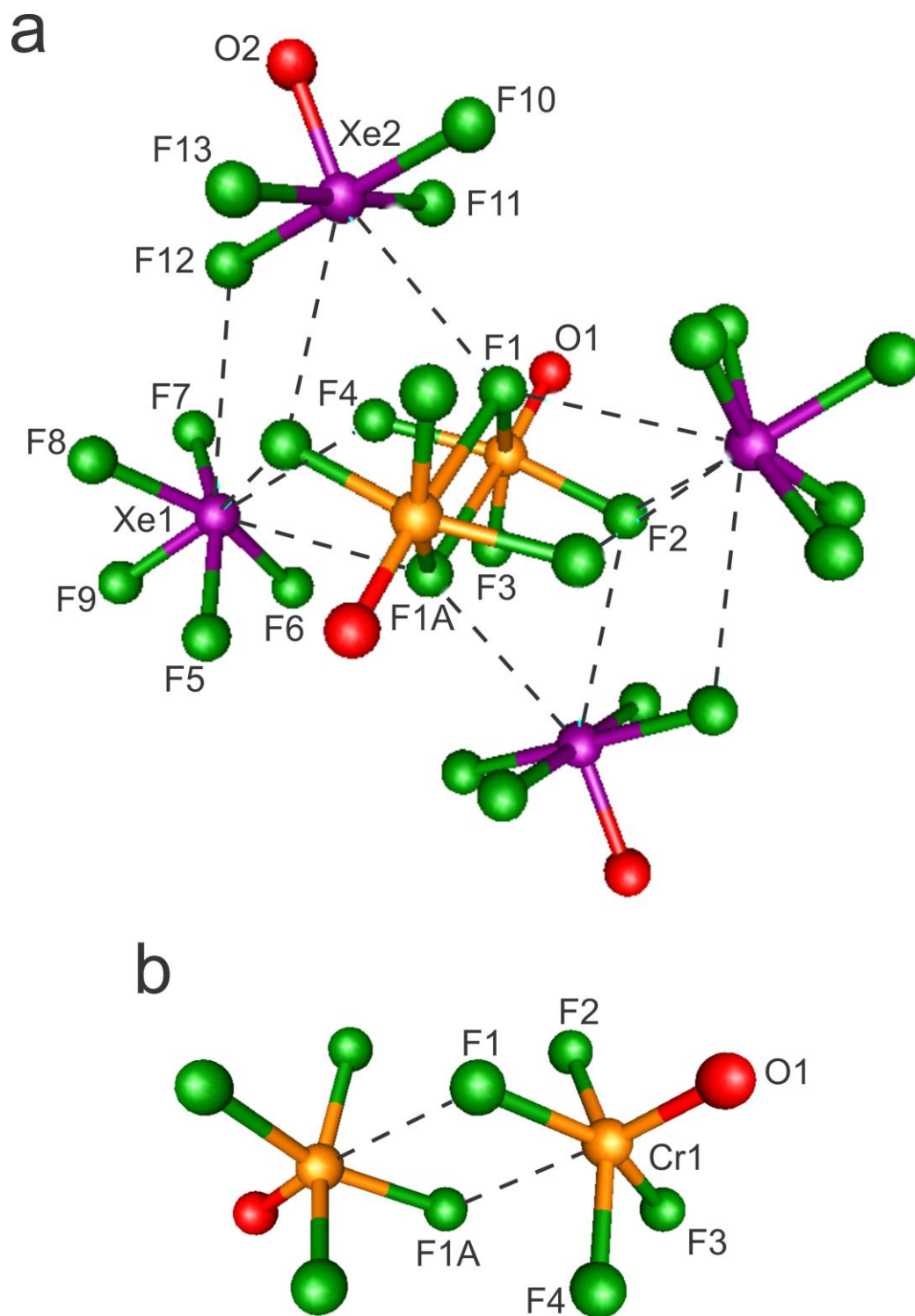
Figure 8. Calculated geometries of (a) $[XeF_5]_2[Cr_2O_2F_8]\cdot 2XeOF_4$ and (b) $[Cr_2O_2F_8]^{2-}$. The PBE1PBE/aug-ccpVDZ(Xe)-Def2-SVP (F, O, Cr) level of theory was used.

[XeF$_5$][Xe$_2$F$_{11}$][CrOF$_5$]·2CrOF$_4$ (*C$_1$*) and [CrOF$_5$]$^{2-}$ (*C$_{4v}$*). The [CrOF$_5$]$^{2-}$ anion optimized to *C$_{4v}$* symmetry, with the Cr−F$_{ax}$ bond slightly longer (1.889 Å) than the Cr−F$_{eq}$ bonds (1.883 Å) (Figure 9). The Cr−O bond (1.559 Å) is also longer than that of the calculated [Cr$_2$O$_2$F$_8$]$^{2-}$ anion (1.523 Å). Unlike [Cr$_2$O$_2$F$_8$]$^{2-}$, the [CrOF$_5$]$^{2-}$ anion of [XeF$_5$][Xe$_2$F$_{11}$][CrOF$_5$]·2CrOF$_4$ severely distorts upon salt formation (Figure 9). The interactions between F$_{ax}$ and Xe$_1$ (2.351 Å), Xe$_2$ (2.752 Å), and Xe$_3$ (3.047 Å) result in significant elongation of the Cr−F$_{ax}$ bond (2.233 Å), which is accompanied by shortening of the Cr−F$_{eq}$ bonds (1.807−1.836 Å), increases in the O−Cr−F$_{eq}$ angles (101.9−102.5° compared to 94.5°), and decreases in the F$_{ax}$−Cr−F$_{eq}$ angles (75.8−80.0° compared to 85.8°). As observed for [XeF$_5$]$_2$[Cr$_2$O$_2$F$_8$]·2XeOF$_4$, the Cr−O bond of [CrOF$_5$]$^{2-}$ (1.491 Å) in [XeF$_5$][Xe$_2$F$_{11}$][CrOF$_5$]·2CrOF$_4$ is significantly shorter than in the gas-phase [CrOF$_5$]$^{2-}$ anion (1.559 Å).

CONCLUSION

The reactions of XeF$_6$ with CrOF$_4$ in melts and in the oxidatively resistant solvents, aHF and CFCl$_3$ resulted in the formation of [XeF$_5$]$_2$[CrF$_6$]·2CrOF$_4$ (**1**), [Xe$_2$F$_{11}$]$_2$[CrF$_6$] (**2**), [XeF$_5$]$_2$[Cr$_2$O$_2$F$_8$] (**3**), [XeF$_5$]$_2$[Cr$_2$O$_2$F$_8$]·2HF (**4**), [XeF$_5$]$_2$[Cr$_2$O$_2$F$_8$]·2XeOF$_4$ (**5**), and [XeF$_5$][Xe$_2$F$_{11}$][CrOF$_5$]·2CrOF$_4$ (**6**), which were characterized by single-crystal X-ray diffraction. The reduction of Cr(VI) to Cr(IV) and Cr(V) occurs by F$_2$ elimination. The reaction of XeF$_6$ with CrOF$_4$ to give [XeF$_5$][Xe$_2$F$_{11}$][CrOF$_5$]·2CrOF$_4$ (6) was shown by low-temperature Raman spectroscopy to proceed through an intermediate salt of the chromium(VI) anion, [CrOF$_5$]$^-$. The syntheses of the aforementioned salts provide the first structural characterizations of the [CrOF$_5$]$^{2-}$ and [Cr$_2$O$_2$F$_8$]$^{2-}$ anions, thereby significantly extending the known oxide fluoride chemistry of Cr(V). The [XeF$_5$]$^+$ and [Xe$_2$F$_{11}$]$^+$ cations of [XeF$_5$]$_2$[CrF$_6$]·2CrOF$_4$ (**1**), [Xe$_2$F$_{11}$]$_2$[CrF$_6$] (**2**), and [XeF$_5$]$_2$[Cr$_2$O$_2$F$_8$] (**3**) interact with the anions and CrOF$_4$ through

Figure 9. Calculated geometries of (a) and (b) [XeF$_5$][Xe$_2$F$_{11}$][CrOF$_5$]·2CrOF$_4$ and (c) [CrOF$_5$]$^{2-}$. The PBE1PBE/aug-ccpVDZ(Xe)-Def2-SVP (F, O, Cr) level of theory was used.

22

Xe---F and Cr---F secondary bonding interactions to give well-separated chains, whereas [XeF$_5$][Xe$_2$F$_{11}$][CrOF$_5$]·2CrOF$_4$ (**6**) and [XeF$_5$]$_2$[Cr$_2$O$_2$F$_8$]·2XeOF$_4$ (**5**) consist of well-isolated formula units that have no significant intermolecular interactions. The [Cr$_2$O$_2$F$_8$]$^{2-}$ anion has C$_i$ symmetry and consists of two symmetry-equivalent [CrOF$_4$]$^-$ anions that interact through two fluorine bridges. The [XeF$_5$]$_2$[Cr$_2$O$_2$F$_8$]·2XeOF$_4$ (**5**) and [XeF$_5$][Xe$_2$F$_{11}$][CrOF$_5$]·2CrOF$_4$ (**6**) salts were also characterized by low-temperature Raman spectroscopy and quantum-chemical calculations were carried out for [XeF$_5$]$_2$[Cr$_2$O$_2$F$_8$]·2XeOF$_4$ (**5**), [Cr$_2$O$_2$F$_8$]$^{2-}$, [XeF$_5$][Xe$_2$F$_{11}$][CrOF$_5$]·2CrOF$_4$ (**6**), and [CrOF$_5$]$^{2-}$ fto obtain their gas-phase optimized geometries, and their vibrational frequency assignments. Other than [OsO$_3$F$_3$]$^-$ and [µ-F(OsO$_3$F$_2$)]$^-$, the [CrOF$_5$]$^{2-}$ and [Cr$_2$O$_2$F$_8$]$^{2-}$ anions provide the only other examples of noble-gas cations that have been stabilized by metal oxide fluoride anions.

EXPERIMENTAL SECTION

Caution! *Anhydrous HF must be handled using appropriate protective gear with easy access to proper treatment procedures[39] in the event of contact with the liquid, vapor, or its solutions. Krypton difluoride, CrOF$_4$, XeF$_6$, [XeF$_5$]$^+$, and [Xe$_2$F$_{11}$]$^+$ are potent oxidative fluorinators and highly energetic materials that are only stable under the rigorously anhydrous conditions employed in the experimental procedures outlined below. All three compounds detonate upon hydrolysis or contact with organic materials. The hydrolysis of XeF$_6$ forms XeO$_3$, a highly endothermic, shock-sensitive detonator when dry, and highly toxic HF. It is therefore imperative that the syntheses of the aforementioned compounds be restricted to small amounts (< 100 mg) and that their syntheses and other manipulations be carried out in FEP (perfluoroethylene/perfluoropropylene copolymer) vessels to avoid sharp fragments in the event of a detonation. The use of adequate protective apparel and shielding are crucial for the*

safe handling of all of these compounds. The utmost precautions must be taken when disposing of these materials and their derivatives.

Apparatus

Manipulations involving air-sensitive compounds were carried out under anhydrous conditions on glass and metal high-vacuum lines and in the inert atmosphere of a dry box as previously described.[39] Syntheses were carried out in reaction vessels constructed from ¼-in. o.d. ($^1/_{32}$-in. wall thickness) lengths of FEP (tetrafluoroethylene-hexafluoropropylene block copolymer) tubing. The tubing was heat-sealed at one end, heat flared at the other end, and connected through a 45° SAE flare nut to the conical end of a Kel-F (chlorotrifluoroethylene polymer) valve to form a compression seal. Reaction vessels and sample tubes were rigorously dried under dynamic vacuum prior to passivation for at least 8 h with 1 atm of F_2 gas for several hours. Vacuum line connections were made using ¼-in. 316 stainless steel Swagelok Ultratorr unions fitted with Viton O-rings.

Materials

Technical grade fluorine gas (98% pure) (Air Products), nitrogen gas (99.995%, H_2O < 0.5 ppm) (Praxair), and high-purity Ar (99.998%, Air Liquide) were used without further purification.

Freon-11 ($CFCl_3$) (Matheson) was dried over P_4O_{10} for several days and distilled into a 175 mL glass dispensing vessel outfitted with a grease-free 6-mm J. Young glass/Teflon stopcock for storage. Small quantities (ca. 0.5 mL) were transferred under static vacuum using a glass vacuum line and a glass Y-piece into individual reaction vessels.

Anhydrous HF (Harshaw Chemicals Co.) was purified as previously described[40] and stored in a Kel-F (polychlorotrifluoroethylene) container equipped with a Kel-Fvalve.

24

Krypton difluoride was prepared by use of a hot wire reactor and purified as previously described[41,42] and stored at −78 °C in dry ice pellets. Small quantities of aHF (ca. 0.1–0.5 mL) were transferred under static vacuum through a previously dried and fluorine passivated FEP manifold.

Xenon hexafluoride was synthesized by heating Xe with F_2 in a 1 : 24 molar ratio under autogenous pressure in a 300 mL nickel vessel to a temperature of 280 °C as previously described.[43] Small amounts of $XeOF_4$ and HF, which likely formed by the reaction of XeF_6 with trace amounts of moisture, were removed by flash distillation under dynamic vacuum at room temperature. Xenon hexafluoride contained small amounts of XeF_4 impurity (<1%), which was converted to XeF_6 by the addition of KrF_2 and melting the bulk solid by slowly heating, with agitation, to 45 °C.

Chromyl fluoride (CrO_2F_2) was prepared by reaction of CrO_3 with MoF_6 according to the published procedure.[1]

Chromium oxide tetrafluoride was synthesized using a modification of a previously reported method.[4] In typical syntheses, 49.7–254.9 mg (0.407–2.090 mmol) of CrO_2F_2 was sublimed into a ¼-in. o.d. FEP reaction vessel. Approximately 0.5 mL of aHF was condensed into the reaction vessel at −196 °C. The frozen HF was melted onto the CrO_2F_2 sample at −78 °C and then refrozen at −196 °C. Krypton difluoride (1–4 equivalents) was sublimed into the reaction vessel at −196 °C followed by warming the mixture to 22 °C, whereupon KrF_2 and CrO_2F_2 reacted over a period of 3 h. The reaction vessel and contents were periodically quenched at −78 °C and vented to remove Kr, O_2, and small amounts of F_2 generated by slow auto decomposition of KrF_2. Over the course of the reaction, the solid and solution color changed from orange-brown to deep red-purple. The progress of the reaction was periodically monitored by LT Raman spectroscopy. Upon completion of the reaction, the Raman spectra

of the product showed large amounts of $KrF_2 \cdot 2CrOF_4$ had crystallized. Pure $CrOF_4$ was obtained by decomposing dry $KrF_2 \cdot CrOF_4$ at 22 °C to Kr, F_2, and $CrOF_4$ over a period of 4 days.

Syntheses and Crystal Growth

[XeF5][Xe2F11][CrOF5]·2CrOF4 **(6).** Inside a dry box, $CrOF_4$ (21.5 mg, 0.149 mmol) was loaded into a passivated ¼-in. FEP reactor equipped with a Kel-F valve maintained at −150 °C by copper plated steel air rifle shot that had been previously cooled inside the cryowell of the dry box. The reaction vessel was then closed and connected to an XeF_6 storage vessel on a high-vacuum metal vacuum line, and 93.0 mg, (0.379 mmol) of XeF_6 was sublimed into the reaction vessel at −196 °C through custom fabricated FEP connections under static vacuum. The solid materials were agitated and allowed to slowly warm to 18 °C, at which point they fused, forming a dark purple liquid that evolved gas for approximately one minute. The reactor was cooled to −196 °C, and the uncondensed volatiles were expanded into an FEP vessel containing a drop of freshly distilled mercury that was also held at −196 °C. When the vessel containing the drop of solid mercury was warmed to −78 °C the surface immediately tarnished, indicating the presence of F_2. Crystals of [XeF5][Xe2F11][CrOF5]·2CrOF4 (**6**) were grown by positioning the reaction vessel nearly horizontally in a shallow water-filled Dewar at 25 °C, which allowed the liquid to spread out into a thin layer. The bath was slowly cooled to 18 °C, whereupon, large needle-shaped, dark red-purple crystals formed. The bath was slowly cooled to 0 °C over a period of 5 h, after which the Raman spectrum was recorded on the crystalline product at −140 °C. The sample was stored at −78 °C. A [XeF5][Xe2F11][CrOF5]·2CrOF4 (**6**) crystal having the dimensions 0.06

26

x 0.13 x 0.13 mm^3 was selected and mounted (*vide infra*) for a low-temperature X-ray structure determination.

[XeF$_5$]$_2$[CrF$_6$]·2CrOF$_4$ (1). A passivated ¼-in o.d. FEP reactor, equipped with a Kel-F valve, was cooled to ca. −150 °C inside a dry box and loaded with CrOF$_4$ (8.8 mg, 0.12 mmol). Xenon hexafluoride (12.3 mg, 0.050 mmol) was sublimed into the reaction vessel at −196 °C under static vacuum to give in a ca. 2:1 molar ratio of CrOF$_4$ to XeF$_6$. The reaction vessel was backfilled with dry nitrogen and allowed to warm to room temperature. A dark red, viscous liquid formed, in which unreacted solid CrOF$_4$ was still present. The reactor was warmed to 60 °C, which resulted in a homogenous dark red solution. Crystals of [XeF$_5$]$_2$[CrF$_6$]·2CrOF$_4$ (**1**) were grown by positioning the reactor in a near-horizontal position in a shallow Dewar filled with water (55 °C) and allowing the molten material to spread out into a thin layer along the length of the reaction tube. The water bath was covered with aluminum foil and allowed to slowly cool to room temperature, whereupon long, dark red-purple needles on the walls of the reactor. The melting point of the crystalline product was ca. 40 °C, which is higher than the melting point of [XeF$_5$][Xe$_2$F$_{11}$][CrOF$_5$]·2CrOF$_4$ (**6**) (ca. 18 °C). This facilitated transfer of the crystalline mass into a passivated FEP reaction tube inside a dry box. A [XeF$_5$]$_2$[CrF$_6$]·2CrOF$_4$ (**1**) crystal having the dimensions 0.04 x 0.05 x 0.16 mm^3 was selected and mounted (*vide infra*) for a low-temperature X-ray crystal structure determination.

[XeF$_5$]$_2$[Cr$_2$O$_2$F$_8$] (3) and [Xe$_2$F$_{11}$][CrF$_6$] (2). Xenon hexafluoride (ca. 100 mg, 4.08 mmol) was transferred under static vacuum into a passivated FEP reaction vessel containing [XeF$_5$]$_2$[CrF$_6$]·2CrOF$_4$ (**1**) (0.082 g, 0.90 mmol). The reactor was warmed to 30 °C and agitated to give a homogeneous, purple-red liquid. The reactor was placed in a water bath at 30 °C and allowed to slowly cool overnight, yielding colorless, needle-shaped crystals of [Xe$_2$F$_{11}$][CrF$_6$] and dark red, block-shaped crystals of [XeF$_5$]$_2$[Cr$_2$O$_2$F$_8$] (**3**). A [Xe$_2$F$_{11}$][CrF$_6$] (**2**)

27

crystal having the dimensions 0.08 x 0.13 x 0.38 mm^3 and a [XeF$_5$]$_2$[Cr$_2$O$_2$F$_8$] (**3**) crystal having the dimensions 0.14 x 0.22 x 0.42 mm^3 were selected and mounted (*vide infra*) for low-temperature X-ray crystal structure determinations. Crystals of [Xe$_2$F$_{11}$]$_2$[CrF$_6$] (**2**), which comprised the majority of the sample, proved difficult to mount because they easily fragmented when manipulated.

[XeF$_5$]$_2$[Cr$_2$O$_2$F$_8$]·2HF (4). Xenon hexafluoride (56.0 mg, 0.223 mmol) was transferred under static vacuum at −196 °C into a passivated FEP reaction vessel containing HF-wetted CrOF$_4$ (ca. 36 mg, 0.25 mmol) in CFCl$_3$ solvent (ca. 0.4 mL). The sample was warmed to room temperature, whereupon CrOF$_4$ and XeF$_6$ rapidly dissolved to give a clear, colorless solution. Pale yellow-green, block-shaped crystals of [XeF$_5$]$_2$[Cr$_2$O$_2$F$_8$]·2HF (**4**), and amber, block-shaped crystals of [XeF$_5$]$_2$[Cr$_2$O$_2$F$_8$]·2XeOF$_4$ (**5**) were grown from the solution at −78 °C over a period of 48 h. A crystal of [XeF$_5$]$_2$[Cr$_2$O$_2$F$_8$]·2HF (**4**), having the dimensions 0.17 x 0.31 x 0.55 mm^3, was selected and mounted (*vide infra*) for a low-temperature X-ray crystal structure determination.

[XeF$_5$]$_2$[Cr$_2$O$_2$F$_8$]·2XeOF$_4$ (5). Using a procedure similar to that used for the synthesis of [XeF$_5$]$_2$[Cr$_2$O$_2$F$_8$]·2HF (**4**), XeF$_6$ (64.5 mg, 0.263 mmol) and CrOF$_4$ (ca. 55 mg, 0.38 mmol) were combined in aHF solvent (ca. 0.4 mL). The sample was warmed to room temperature, whereupon CrOF$_4$ and XeF$_6$ rapidly dissolved to give an amber solution. Amber, block-shaped crystals of [XeF$_5$]$_2$[Cr$_2$O$_2$F$_8$]·2XeOF$_4$ (**5**) were grown from solution overnight at −78 °C. A Raman spectrum was recorded on the dry crystalline sample at −150 °C. A crystal having the dimensions 0.13 x 0.17 x 0.21 mm^3 was selected and mounted (*vide infra*) for a low-temperature X-ray crystal structure determination.

X-ray Crystallography

Crystal Mounting Procedure. Crystalline samples were stored at −78 °C until a suitable crystal could be selected and mounted on the diffractometer using a previously described low-temperature crystal mounting procedure.[39] Crystals were rapidly dumped from the reaction vessel under a dry nitrogen or argon flow into an aluminum trough which was cooled to −100 ±5°C by means of a cold stream of dry N_2 gas. The cold trough allowed individual crystals to be manipulated under a stereomicroscope. Single crystals were mounted at the tip of a glass fiber or dual-thickness polymer loop (MiTeGen, Ithaca, NY; MicroMount;™ 100–500 μm) at −100 °C using perfluoropolyether oil (Fomblin Z-25) as the adhesive and were transferred to the diffractometer using cryotongs (Hampton Research) which had been cooled to −196 °C in liquid N_2.

Collection and Reduction of X-ray Data. Crystals were centered on a Bruker SMART APEX II diffractometer equipped with an APEX II 4K CCD (charge-coupled device) area detector and a triple-axis goniometer that was controlled by the APEX II Graphical User Interface (GUI) software.[44] A Bruker Triumph curved crystal monochromator was used with a Mo Kα (λ = 0.71073 Å) radiation source for all compounds. Diffraction data collection at −173 °C consisted of ω- and φ-scans collected at 0.5º intervals. The crystal-to-detector distance was 4.954 cm for (**1**)–(**3**), (**6**), and 4.960 cm for (**4**), (**5**), and data collection was carried out in a 512 x 512 pixel mode using 2 x 2 pixel binning. The raw data sets were processed by use of the APEX III GUI software.[45] The SADABS[46] program was used for scaling the diffraction data.

Solution and Refinement of the Structure. The XPREP program[47] was used to confirm unit cell dimensions and the crystal lattice. All calculations were carried out using the SHELXTLplus[47] and the Olex2[48] packages for structure determination, solution refinement,

and molecular graphics. The space group choice was confirmed using Platon.[49] The final refinement was obtained by introducing anisotropic thermal parameters and the recommended weightings for all of the atoms except the hydrogen atoms, which were placed at locations derived from a difference map. The maximum electron density in the final difference Fourier map was located near the xenon atom.

CSD XXXX–XXXX contain supplementary crystallographic data for this paper. These data may be obtained free of charge from FIZ Karlsruhe, Germany.

Raman Spectroscopy

The Raman spectrum was recorded on a Bruker RFS 100 FT-Raman spectrometer using 1064-nm excitation, 300 mW laser power, and ± 0.5 cm^{-1} resolution on samples in ¼-in. o.d. FEP vessels as previously described.[39]

Computational Details

Density-functional theory (DFT) was employed to study the electronic structures of $[XeF_5]_2[Cr_2O_2F_8] \cdot 2XeOF_4$, $[Cr_2O_2F_8]^{2-}$, $[XeF_5][Xe_2F_{11}][CrOF_5] \cdot 2CrOF_4$, and $[CrOF_5]^{2-}$. All basis sets were obtained online from the EMSL Basis Set Exchange (https://bse.pnl.gov/bse/portal).[50] Quantum-chemical calculations were carried out using the program Gaussian 09[51] for geometry optimizations and to create wavefunction files. The GaussView[52] program was used to visualize the vibrational displacements that form the basis for the vibrational mode descriptions.

Supporting Information

The Supporting Information for the paper follows.

Acknowledgements

Conflict of Interest

The authors declare no conflict of interest.

Key Words

Chromium oxide fluorides • Xenon(VI) chemistry • X-ray crystallography • Raman spectroscopy • Quantum-chemical calculations

References

1.   P. J. Green, G. L. Gard, *Inorg. Chem.* **1977**, *16*, 1243–1245.

2.   E. G. Hope, P. J. Jones, W. Levason, J. S. Ogden, M. Tajik, J. W. Turff, *J. Chem. Soc., Dalton Trans.* **1985**, *3*, 529–533.

3.   K. O. Christe, W. W. Wilson, R. A. Bougon, *Inorg. Chem.* **1986**, *25*, 2163–2169.

4.   H. P. A. Mercier, D. S. Brock, U. Breddeman, G. J. Schrobilgen, *to be submitted for publication.*

5.   O. Glemser, H. Roesky, K. H. Hellberg, *Angew. Chem. Int. Ed. Engl.* **1963**, *2*, 266−267.

6.   E. G. Hope, P. J. Jones, W. Levason, J. S. Ogden, M. Tajik, J. W. Turff, *J. Chem. Soc., Dalton Trans.* **1985**, *7*, 1443−1449.

7.   E. Jacob, H. Willner, *Chem. Ber.* **1990**, *123*, 1319−1321.

8.   J. Jacobs, H. S. P. Müller, H. Willner, E. Jacob, H. Bürger, *Inorg. Chem.* **1992**, *31*, 5357−5363.

9.   T. Schlöder, F. Brosi, B. J. Freyh, T. Vent-Schmidt, S. Riedel, *Inorg. Chem.* **2014**, *53*, 5820−5829.

10.   A. J. Edwards, *Proc. Chem. Soc., London* **1963**, 205.

11.   A. Beuter, W. Sawodny, *Z. Anorg. Allg. Chem.* **1976**, *427*, 37−44.

12.   R. Bougon, T. Bui Huy, P. Charpin, *Inorg. Chem.* **1975**, *14*, 1822−1830.

13.   T. Kanatani, K. Matsumoto, R. Hagiwara, *Eur. J. Inorg. Chem.* **2010**, 1049−1055.

14.   S. P. Mallela, J. M. Shreeve, *Organometallics* **1989**, *8*, 2751−2754.

15.   P. J. Green, B. M. Johnson, T. M. Loehr, G. L. Gard, *Inorg. Chem.* **1982**, *21*, 3562−3565.

16.   M. McHughes, R. D. Willett, H. B. Davis, G. L. Gard, *Inorg. Chem.* **1986**, *25*, 426−427.

17.   H. C. Clark, Y. N. Sadana, *Can. J. Chem.* **1964**, *42*, 702−704.

18.   E. G. Hope, P. J. Jones, W. Levason, J. S. Ogden, M. Tajik, J. W. Turff, *J. Chem. Soc., Dalton Trans.* **1984**, *11*, 2445−2447.

19.   P. T. Manoharan, M. T. Rogers, *J. Chem. Phys.* **1968**, *49*, 5510−5519.

20.   R. J. Gillespie, B. Landa, G. J. Schrobilgen, *J. Inorg. Nucl. Chem.* **1976**, 179−182, Supplement.

21.   M. J. Hughes, H. P. A. Mercier, G. J. Schrobilgen, *Inorg. Chem.* **2010**, *49*, 3501–3515.

22.   K. Lutar, H. Borrmann, B. Žemva, *Inorg. Chem.* **1998**, *37*, 3002–3006.

23.   K. Leary, A. Zalkin, N. Bartlett, *Inorg. Chem.* **1974**, *13*, 775−779.

24. S. Hoyer, T. Emmler, K. Seppelt, *J. Fluorine Chem.* **2006**, *127*, 1415–1422.

25. R. J. Gillespie, I. Hargittai In *The VSEPR Model of Molecular Geometry*; Allyn and Bacon: Boston, M. A. 1991; pp 40−61.

26. N. Bartlett, M. Gennis, D. D. Gibler, B. K. Morrell, A. Zalkin, *Inorg. Chem.* **1973**, *12*, 1717–1721.

27. N. Bartlett, F. Einstein, D. F. Stewart, J. Trotter, *J. Chem. Soc. (A),* **1967**, *0*, 1190–1193.

28. A. Bondi, *J. Phys. Chem.* **1964**, *68,* 441–451.

29. K. Leary, D. H. Templeton, A. Zalkin, N. Bartlett, *Inorg. Chem.* **1973**, *12*, 1726–1730.

30. N. Bartlett, B. G. DeBoer, F. J. Hollander, F. O. Sladky, D. H. Templeton, A. Zalkin, *Inorg. Chem.* **1974,** *13*, 780–785.

31. A. Jesih, K. Lutar, I. Leban, B. Zemva, *Eur. J. Solid State Inorg. Chem.* **1991**, *28*, 829–840.

32. B. E. Pointner, R. J. Suontamo, G. J. Schrobilgen, *Inorg. Chem.* **2006**, *45*, 1517–1534.

33. K. Lutar, A. Jesih, I. Leban, B. Zemva, N. Bartlett, *Inorg. Chem.* **1989**, *28*, 3467–3471.

34. A. Jesih, K. Lutar, I. Leban, B. Zemva, *Inorg. Chem.* **1989**, *28*, 2911–2914.

35. M. J. Hughes, D. S. Brock, H. P. A. Mercier, G. J. Schrobilgen, *J. Fluorine Chem.* **2011**, *132*, 660–668.

36. Z. Mazej, E. Goreshnik, *Eur. J. Inorg. Chem.* **2008**, *11*, 1795–1812.

37. Z. Mazej, E. Goreshnik, *Eur. J. Inorg. Chem.* **2017**, *21*, 1795–1812.

38. W. G. Fateley, F. R. Dollish, N. T. McDevitt, F. F. Bentley, Infrared and Raman Selection Rules for Molecular and Lattice Vibrations: The Correlation Method, Wiley & Sons, New York, **1972**.

39. W. J. Casteel, D. A. Dixon, H. P. A. Mercier, G. J. Schrobilgen, *Inorg. Chem.* **1996**, *35*, 4310−4322.

40. A. A. A. Emara, G. J. Schrobilgen, *Inorg. Chem.* **1992**, *31*, 1323–1332.

41. J. F. Lehmann, D. A. Dixon, G. J. Schrobilgen, *Inorg. Chem.* **2001**, *40*, 3002–3017.

42. J. F. Lehmann, H. P. A. Mercier, G. J. Schrobilgen, *Coord. Chem. Rev.* **2002**, *233–234*, 1–39.

43. J. G. Malm, C. L. Chernick, *Inorg. Synth.* **1966**, *8*, 258–260.

44. APEX2, release v2014.9-0; Bruker AXS Inc.: Madison, WI, **1995**.

45. APEX3, release v2017.3-0; Bruker ACS Inc.: Madison, WI, **1995**.

46. G. M. Sheldrick, SADABS (Siemens Area Detector Absorption Corrections), version 2.03; Siemens Analytical X-ray Instruments, Inc.: Madison, WI, **1999**.

47. G. M. Sheldrick, SHELXTL-Plus, release 5.1; Siemens Analytical X-ray Instruments, Inc.: Madison, WI, **1998**.

48. O. V. Dolomanov, L. J. Bourhis, R. J. Gildea, J. A. K. Howard, J. Puschmann, *J. Appl. Crystallogr.* **2009**, *42*, 339–341.

49. A. L. Spek, *J. Appl. Crystallogr.* **2003**, *36*, 7–13.

50. Basis sets were obtained from the Extensible Computational Chemistry Environment Basis set Database, version 2/25/04, as developed and distributed by the Molecular Science Computing Facility, Environmental and Molecular Science Laboratory, which is part of the Pacific Northwest Laboratory, P.O. Box 999, Richland, WA, 99352.

51. M. J. Frisch, G. W. Trucks, H. B. Schlegel, G. E. Scuseria, M. A. Robb, J. R. Cheeseman, G. Scalmani, V. Barone, B. Mennucci, G. A. Petersson, H. Nakatsuji, M. Caricato, X, Li, H. P. Hratchian, A. F. Izmaylov, J. Bloino, G. Zheng, J. L. Sonnenberg, M. Hada, M. Ehara, K. Toyota, R. Fukuda, J. Hasegawa, M. Ishida, T. Nakajima, Y.

Honda, O. Kitao, H. Nakai, T. Vreven, J. A. Jr. Montgomery, J. E. Peralta, F. Ogliaro, M. Bearpark, J. J. Heyd, E. Brothers, K. N. Kudin, V. N. Staroveroc, R. Kobayashi, J. Normand, K. Raghavachari, A. Rendell, J. C. Burant, S. S. Lyengar, J. Tomasi, M. Cossi, N. Rega, N. J. Milliam, M. Klene, J. E. Knox, J. B. Cross, V. Bakken, C. Adamo, J. Jaramillo, R. Gomperts, R. E. Stratmann, O. Yazyev, A. Austin, R. Cammi, C. Pomelli, J. W. Ochterski, R. L. Martin, K. Marokuma, V. G. Zakrzewski, G. A. Voth, P. Salvador, J. J. Dannenberg, S. Dapprich, A. Daniels, D. Farkas, J. Foresman, J. V. Ortiz, J. Cioslowski, D. J. Fox, Gaussian 09, Revision D.01; Gaussian, Inc: Wallingford, CT, **2009**.

52.   GaussView, version 3.0; Gaussian Inc.: Pittsburgh, PA, **2003**.

Entry for the Table of Contents

XeF$_6$ and Cr^{VI}OF$_4$ react to form [XeF$_5$]$^+$ and [Xe$_2$F$_{11}$]$^+$ salts of the [Cr^{IV}F$_6$]$^{2-}$, [Cr^{V}OF$_5$]$^{2-}$, and [Cr$^V_2$O$_2$F$_8$]$^{2-}$ salts. The salts have been structurally characterized by single-crystal X-ray diffraction and [CrOF$_5$]$^-$ was identified as a reaction intermediate by Raman spectroscopy.

[XeF$_5$][Xe$_2$F$_{11}$][Cr^{V}OF$_5$]·2CrOF$_4$ [XeF$_5$]$_2$[Cr$^V_2$O$_2$F$_8$]·2XeOF$_4$
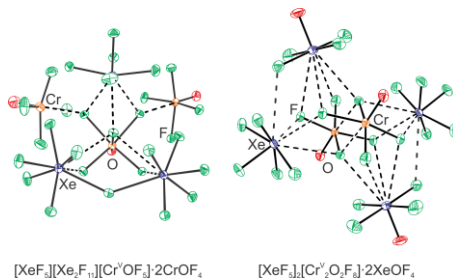
*Daniel G. Stuart, Mark R. Bortolus, James T. Goettel, Hélène P. A. Mercier, Gary J. Schrobilgen **

Page No. – Page No.

Chromium Oxide Tetrafluoride and Its Reactions with Xenon Hexafluoride; the [XeF$_5$]$^+$ and [Xe$_2$F$_{11}$]$^+$ Salts of the [Cr^{VI}OF$_5$]$^-$, [Cr^{IV}F$_6$]$^{2-}$, [Cr^{V}OF$_5$]$^{2-}$, and [Cr$^V_2$O$_2$F$_8$]$^{2-}$ Anions